



PAPER

OPEN ACCESS

RECEIVED
2 October 2019REVISED
7 November 2019ACCEPTED FOR PUBLICATION
8 January 2020PUBLISHED
17 January 2020

Original content from this work may be used under the terms of the [Creative Commons Attribution 3.0 licence](https://creativecommons.org/licenses/by/4.0/).

Any further distribution of this work must maintain attribution to the author(s) and the title of the work, journal citation and DOI.



Relation between solutions of the Schrödinger equation with transitioning resonance solutions of the gravitational three-body problem

Edward Belbruno^{1,2} ¹ Department of Mathematics, Yeshiva University, New York, NY, United States of America² Department of Astrophysical Sciences, Princeton University, Princeton, NJ, United States of AmericaE-mail: Edward.Belbruno@yu.edu**Keywords:** celestial mechanics, resonance transition, Schrodinger equation, three-body problem

Abstract

It is shown that a class of approximate resonance solutions in the three-body problem under the Newtonian gravitational force are equivalent to quantized solutions of a modified Schrödinger equation for a wide range of masses that transition between energy states. In the macroscopic scale, the resonance solutions are shown to transition from one resonance type to another through weak capture at one of the bodies, while in the Schrödinger equation, one obtains quantized wave solutions transitioning between different energies. The resonance transition dynamics provides a classical model of a particle moving between different energy states in the Schrödinger equation. This methodology provides a connection between celestial and quantum mechanics.

1. Introduction

The purpose of this paper is to describe a mechanism to globally model the solutions of a modified Schrödinger equation and how they transition between energy states, with a special set of approximate resonance solutions to the classical gravitational Newtonian three-body problem, for a wide range of masses. These resonance solutions transition from one resonance to another through the process of weak capture.

We consider a special version of the three-body problem that has proved to be useful in understanding the complexities of three-body motion, in the macroscopic scale, going back to Poincaré [1]. This is the circular restricted three body-problem, where the motion of one body, P_0 , is studied as it moves under the influence of the gravitational field of P_1 , P_2 , assumed to move in mutual circular orbits of constant frequency ω . It is also assumed that the mass of P_0 , labeled m_0 , is negligible with respect to the masses of P_1 , P_2 , labeled m_1 , m_2 , respectively. In this paper, we will also assume that m_2 is much smaller than m_1 , $m_2 \ll m_1$. For example, in the case of planetary objects, one can take P_1 , P_2 to be the Earth, Moon, respectively, and P_0 to be a rock. One can scale down m_0 , m_1 , m_2 , as well as the relative distances between the particles, until the quantum scale is reached where the pure gravitational modeling is no longer sufficient. When using a rotating coordinate system that rotates about the center of mass of P_1 , P_2 with constant frequency ω , it is well known that Hamiltonian function for the motion of P_0 is time independent defining a conservative system (see section 3).

For a general class of conservative systems, that includes, for example, the restricted three-body problem considered here, it is known that such systems can be associated to the Schrödinger equation. As is described in Lanczos [2], this can be done by computing the action function $S(x)$ for the motion of P_0 , where x is the position of P_0 .¹ S is a solution of the Hamilton-Jacobi partial differential equation associated to the restricted three-body problem. The $x(t)$ are orthogonal to the surface $S(x) = C$, for constant C . In this sense, the iso- S surfaces locally determine the trajectories $x(t)$, that is for t having sufficiently small variation. On the other hand, it can be shown that S is the phase of wave solutions to the Schrödinger equation. Thus, $S(x) = C$ is a wave surface.

¹ S is obtained as the integral of the Lagrangian function $L(x, y)$, $y = dx/dt$, over minimizing trajectories $x(t)$.

Conversely, starting with the S satisfying the Schrödinger equation, one obtains the Hamiltonian-Jacobi equation provided the Planck's constant $\hbar \rightarrow 0$. This equivalence is local since in general S can only be shown to locally exist as a solution to the Hamiltonian-Jacobi equation, which is the case for the three-body problem. For the full equivalence it is necessary that one restricts $\hbar \rightarrow 0$ that is not realistic. More significantly, this equivalence does not determine the global behavior of the solutions $x(t)$ and how they dynamically can model the transition of energy states for solutions of the Schrödinger equation.

This paper will use methods of dynamical systems to globally determine special resonance motions for P_0 that are shown to be equivalent to different energy states for a modified Schrödinger equation and where the transition between energy states is equivalent to the process of weak capture in the three-body problem described in this paper. This result does not require the restriction of Planck's constant, and doesn't use Planck's constant in the modeling. The action function S is not used. Due to the complexity of the motions described, it is seen that using the iso- S surfaces to locally determine the global solutions would not seem feasible.

We describe a mechanism for the existence of a special family, \mathfrak{F} , of approximate resonance motions of P_0 about P_1 , that transition from one resonance to another by the process of *weak capture* by P_2 . This is a temporary capture defined in section 2. These motions are approximately elliptical with frequency $\omega_1 \equiv \omega_1(m/n)$. $\omega_1(m/n)(t)$ or equivalently $\omega_1(t)$, are functions of the time t , where $\omega_1(m/n)$ is approximately equal to the constant values $(m/n)\omega$, m , n are positive integers. That is, the period of motion of P_0 is approximately synchronized with the circular motion of P_2 about P_1 , where in the time P_0 makes approximately n revolutions about P_1 , P_2 makes m revolutions about P_1 . The approximate resonance value of the frequency means that $|\omega_1(t) - (m/n)\omega| < \delta$, for a small tolerance δ as time varies for restricted time spans, described in section 2. When P_0 is moving on an approximate resonance orbit about P_1 , it will eventually move away from this orbit and become captured temporarily about P_2 , in weak capture. When P_0 escapes from this capture, it again moves about P_1 in another resonance elliptical orbit, with approximate resonance m'/n' . This process repeats either indefinitely, or ends when, for example, P_0 escapes the P_1, P_2 -system. This also implies that the approximate two-body energy E_1 of P_0 about P_1 can only take on a discrete set of values, $E_1(m/n)(t)$ at each time t , which are approximately constant defined by the resonances. This is stated as result A in section 2 and as theorem A in section 3. The properties and dynamics of weak capture, and weak escape, are described section 3. Comets can perform such resonance transitions(see sections 2 3).

A modified Schrödinger equation is defined for the motion of P_0 about P_1 , under the gravitational perturbation of P_2 . This is first considered in the case of macroscopic masses. It is given by,

$$-\frac{\sigma^2}{2\nu}\nabla^2\Psi + \bar{V}\Psi = E\Psi, \quad (1)$$

where $\nabla^2 \equiv \nabla \cdot \nabla$ is the Laplacian operator, \bar{V} is an averaged three-body gravitational potential, E is the energy, and ν is the reduced mass for P_0, P_1 . σ is a function that depends on m_0, m_1 and G , the gravitational constant. σ replaces $\hbar = h/2\pi$, h is Planck's constant that is in the classical Schrödinger equation. In this case, for macroscopic values of the masses, since P_0 is not a wave, Ψ is used to determine the probability distribution function, $|\Psi|^2$, of locating P_0 near P_1 as a macroscopic body. We show in section 4 that E can only take on the following approximate quantized values,

$$E_{\tilde{n}} = -\frac{4\sigma}{\tilde{n}^2}, \quad (2)$$

$\tilde{n} = 1, 2, 3, \dots$ As seen in section 2, this implies that the frequency of P_0 takes a particularly simple form that is independent of any parameters. These frequencies have the approximate values, $8/\tilde{n}^3$. Ψ is explicitly computed in section 4. $|\Psi|^2$ is shown to be exponentially decreasing as a function of the distance of P_0 from P_1 . The general solution, Ψ , of the modified Schrödinger equation is described in result B in section 2.

A main result of this paper is that the quantized energy values $E_{\tilde{n}}$ correspond to a subset, \mathfrak{U} , of the resonance orbit family, \mathfrak{F} , of P_0 about P_1 . This is listed as result C in section 2. This provides a global equivalence of the solutions of the modified Schrödinger equation with the transitioning resonance solutions of the the three-body problem.

As a final result, we show is that the solution, Ψ , for the location of P_0 for the modified Schrödinger equation for the macroscopic values of the masses, can be extended into the quantum-scale. This is summarized as result D in section 2. This gives a way to mathematically view the resonance motions in the quantum-scale, as an extension of the resonance solutions for macroscopic particles. Other models, such as the classical Schrödinger and Schrödinger-Newton equations are given in latter sections.

The results of this paper are described in detail and summarized in section 2. This section contains the main findings of this paper. Additional details, derivations, and proofs are contained in section 3 for weak capture and in section 4 for the modified Schrödinger equation.

2. Summary of results, definitions and assumptions

In this section we elaborate on the results described in the Introduction. The first set of results pertain to a family of resonance orbits about P_1 obtained from the three-body problem and the second set of results pertain to finding these orbits using a modified Schrödinger equation.

2.1. Resonance orbits in the three-body problem and weak capture

The motion of P_0 is defined for the circular restricted three-body problem described in the Introduction. It is sufficient to use the planar version of this model, without loss of generality for the purposes of this paper, where P_0 moves in the same plane of motion as that of the uniform circular motion of P_1, P_2 of constant frequency ω (see section 3). The macroscopic masses satisfy, $m_2/m_1 \ll 1$ and the mass of m_0 is negligibly small so that P_0 does not gravitationally perturb P_1, P_2 , but P_1, P_2 perturb the motion of P_0 . We consider an inertial coordinate system, $(X_1, X_2) \in \mathbb{R}^2$, whose origin is the center of mass of P_1, P_2 .

The differential equations for P_0 are given by the classical system

$$\dot{X} = \Omega_X(X, t), \quad (3)$$

where $X = (X_1, X_2) \in \mathbb{R}^2, t \in \mathbb{R}^1, \dot{\cdot} \equiv \frac{d}{dt}, \Omega_X \equiv (\Omega_{X_1}, \Omega_{X_2}) (\Omega_X \equiv \partial\Omega/\partial X)$ and

$$\Omega = \frac{Gm_1}{r_1(t)} + \frac{Gm_2}{r_2(t)} \quad (4)$$

where $r_1(t) = |X - a_1(t)|, r_2 = |X - a_2(t)|, |\cdot|$ is the standard Euclidean norm. The mutual circular orbits of P_1, P_2 are given by $a_1(t) = \rho_1(\cos \omega_a t, \sin \omega_a t), a_2(t) = -\rho_2(\cos \omega_b t, \sin \omega_b t)$, with constant circular frequencies ω_a, ω_b of P_1, P_2 , respectively. We have divided both sides of (3) by m_0 and then took the limit as $m_0 \rightarrow 0$. It is well known that the solutions of the circular restricted three-body problem for P_0 accurately model the motion of P_0 in the general three-body problem for circular initial conditions for P_1, P_2 , with m_0 kept positive and negligibly small.

It is noted that all solutions $\xi(t) = (X(t), \dot{X}(t)) \in \mathbb{R}^4$ considered in this study will be C^∞ in both t and initial conditions, $\xi(t_0) = (X(t_0), \dot{X}(t_0))$ at an initial time t_0 . We refer to C^∞ as *smooth* dependence. More exactly, this means that all derivatives of $\xi(t)$ with respect to t of all orders are continuous and all partial derivatives of $\xi(t, \xi(t_0))$ with respect to $X_1(t_0), X_2(t_0), \dot{X}_1(t_0), \dot{X}_2(t_0)$, of all orders, are continuous.

Although m_0 is taken in the limit to be 0 in the definition of the differential equations for the motion of P_0 , we will assume it is non-zero but still negligible in mass with respect $P_1, P_2, m_0 \gtrsim 0$, in all equations that follow.

We transform to a P_1 -centered coordinate system for the restricted three-body problem. In this system, P_2 moves about P_1 at a constant distance β , with constant circular frequency $\omega = \sqrt{G(m_1 + m_2)/\beta}$. Before stating our first result, two definitions are needed.

Assuming m_2 is much smaller than m_1 , when P_0 moves about P_1 with elliptic initial conditions at an initial time $t = t_0$, this elliptic motion will be slightly perturbed by P_2 ². Let a_1 be the semi-major axis of P_0 with respect to P_1 . As a function of time, a_1 will vary. If $m_2 = 0$, then a_1 is constant since P_0 will move on a pure ellipse. If m_2 is small, then P_0 moves in a nearly elliptic orbit about P_1 , and $a_1(t)$ will be nearly constant for restricted time spans. This orbital element, along with the eccentricity, $e_1(t)$, true anomaly, $\theta_1(t)$, and other orbital elements, can be calculated for each t using the variational differential equations obtained from (3). (see [3–6]). These are referred to as *osculating elements*. e_1 will likewise be nearly constant for a nearly elliptical orbit of P_0 about P_1 .

The variation of the frequency $\omega_1(t)$ can be obtained from $a_1(t)$: The osculating two-body period, T_1 , of P_0 is explicitly related to $a_1(t)$ by Kepler's Third Law, $a_1^3 = (2\pi)^{-2} T_1^2 G(m_0 + m_1)$, and $\omega(t) = T_1^{-1}$.

Definition 1. An approximate resonance orbit, $\Phi_{m/n}(t)$, of P_0 moving about P_1 in a P_1 -centered coordinate system, $Y = (Y_1, Y_2)$, as a function of t in resonance with P_2 , is an approximate elliptical orbit of frequency $\omega_1 = \omega_1(t)$, where $\omega_1 \approx (m/n)\omega$. m, n are positive integers. Thus, ω_1 is approximately constant as time varies. In phase space, $(Y, \dot{Y}) \in \mathbb{R}^4, \Phi_{m/n}(t) = (Y_1(t), Y_2(t), \dot{Y}_1(t), \dot{Y}_2(t))$. $\Phi_{m/n}(t)$ has a period $T_1 = \omega_1^{-1}$, approximately constant. $T_1 \approx (n/m)T, T$ is the constant circular period of P_2 about $P_1, T = \omega^{-1}$. For notational purposes, we refer to an approximate resonance orbit as a resonance orbit for short. A resonance orbit with $\omega_1 \approx (m/n)\omega$ is also referred to as a $n:m$ resonance orbit. (*Nearly resonant* motion, related to approximate resonance motion, is described in [7].)

The term 'approximate' in definition 1 means to within a small tolerance, $\mathcal{O}(\delta), \delta = m_2/m_1 \ll 1$. $\mathcal{O}(\delta)$ is a function of time, t , and smooth in t . An approximate elliptical orbit means that the variation of the orbital parameters (ω_1, a_1, e_1) of $\Phi(t) = (Y(t), \dot{Y}(t))$, with respect to P_1 in a P_1 -centered coordinate system, will slightly

² By the Kolmogorov-Arnold-Moser Theorem, the motion will stay approximately elliptic for all time for many initial conditions [1].

vary by $\mathcal{O}(\delta)$ due to the gravitational perturbation of P_2 . The two-body energy of $\Phi_{m/n}(t)$ with respect to P_1 is labeled, $E_1(m/n) = E_1(m/n)(t)$, which is approximately constant. Note that the general Kepler energy $E_1(t)$ along a trajectory $(Y(t), \dot{Y}(t))$ is given by (7).

Thus, $\omega_1 \approx (m/n)\omega$ is equivalent to $\omega_1 = (m/n)\omega + \mathcal{O}(\delta)$. a_1, e_1 likewise vary within a variation $\mathcal{O}(\delta)$. The variations $\mathcal{O}(\delta)$ are all different functions for the different parameters, but the same notation is used. The tolerance on these orbital parameters is valid for finite times. We assume that t varies over finite time spans. Thus, for a given variable, say $\omega_1(t)$, if $\epsilon_1 > 0$ is a given number, and $t \in [t_0, t_1], t_1 > t_0, m_2$ can be taken small enough so that $|\mathcal{O}(\delta)| < \epsilon_1$

For a resonance orbit to be well defined, it is assumed that $m_2 > 0$. If $m_2 = 0$, then even though ω is defined, P_2 no longer exists. Thus, we assume $m_2 > 0$ throughout this paper, unless otherwise indicated. This assumption is also necessary for the definition of weak capture.

We define ‘weak capture’ of P_0 about P_2 . In this case, we change to a P_2 -centered coordinate system. This type of capture is discussed in section 3. Weak capture is where the two-body energy, E_2 , of P_0 with respect to P_2 is temporarily negative. It is used to define an interesting region about P_2 described in the next section called the weak stability boundary. Chaotic motion occurs on and near this region.

Definition 2. P_0 has *weak capture* about P_2 , in a P_2 -centered coordinate system, $Z = (Z_1, Z_2)$, at a time t_0 if the two-body energy, E_2 , of P_0 with respect to P_2 , is negative at t_0 and for a finite time after where it becomes positive (P_0 escapes). More precisely, E_2 is given by

$$E_2 = \frac{1}{2}|\dot{Z}|^2 - \frac{G(m_0 + m_2)}{r_2}, \tag{5}$$

$r_2 = |Z| > 0$. Let $\mathcal{Z}(t) = (Z_1(t), Z_2(t), \dot{Z}_1(t), \dot{Z}_2(t))$ be a solution for the differential equations (3) in P_2 -centered coordinates for $t \geq t_0$. P_0 is weakly captured at t_0 if $E_2(\mathcal{Z}(t)) < 0$ for $t_0 \leq t < t_1, t_0 < t_1, E_2(\mathcal{Z}(t_1)) = 0, E_2(\mathcal{Z}(t)) \gtrsim 0$ for $t \gtrsim t_1$. After P_0 leaves weak capture at t_1 , we say that P_0 has *weak escape* from P_2 at $t = t_1$. Weak capture in backwards time from t_0 is similarly defined.

P_0 is *captured* at a point $(Z_1(t), Z_2(t))$ of a trajectory $\mathcal{Z}(t)$ at t^* if $E_2(\mathcal{Z}(t^*)) < 0$. Capture at a point need not imply weak capture, in forward time, since P_0 could be captured for all time $t > t^*$.

This dynamics is summarized in result A and proven in section 3, where it is formulated more precisely as Theorem A.

Result A. Weak capture of P_0 about P_2 at a time t_0 yields resonance motion of P_0 about P_1 , which repeats yielding a family, \mathfrak{F} , of resonance orbits. More precisely,

Assume P_0 is weakly captured by P_2 at time $t = t_0$, then

- (i) As t increases from t_0 , P_0 first escapes from P_2 and then P_0 moves onto a resonance orbit, $\Phi_{m/n}(t)$, about P_1 . P_0 performs a finite number of cycles about P_1 until it eventually moves again to weak capture by P_2 , where the process continues and P_0 moves onto another resonance orbit. When P_0 moves from $\Phi_{m/n}(t)$ to another resonance orbit, $\Phi_{m'/n'}(t)$, m', n' may or may not equal m, n . In general, a sequence of resonance orbits is obtained, $\{\Phi_{m/n}(t), \Phi_{m'/n'}(t), \dots\}$. The process stops when P_0 escapes the $P_1 P_2$ -system, collides with P_2 or moves away from a resonance frequency. This set of resonance orbits forms a family, \mathfrak{F} , of orbits, that depend on the initial weak capture condition.
- (ii) When P_0 moves onto a sequence of resonance orbits about P_1 as described in (i), then a discrete set of energies are obtained, $\{E_1(m, n), E_1(m', n'), \dots\}$.

The transitioning of $\Phi_{m/n}(t)$ to $\Phi_{m'/n'}(t)$ is shown in a sketch in figure 1.

The proof of theorem A is given in detail in section 3.

Applications of theorem A to comet motions and numerical simulations is described in section 3.

A key result obtained in section 3 is,

Lemma A. The frequency $\omega_1(m/n)(t)$ of $\Phi_{m/n}(t)$ is given by,

$$\omega_1(m/n) = (m/n)\omega + \mathcal{O}(\delta), \tag{6}$$

where $\mathcal{O}(\delta)(t)$ is smooth in t .

(i) Is proven in section 3 as theorem A. We prove (ii): consider the general two-body energy of P_0 with respect to P_1 . It is given by,

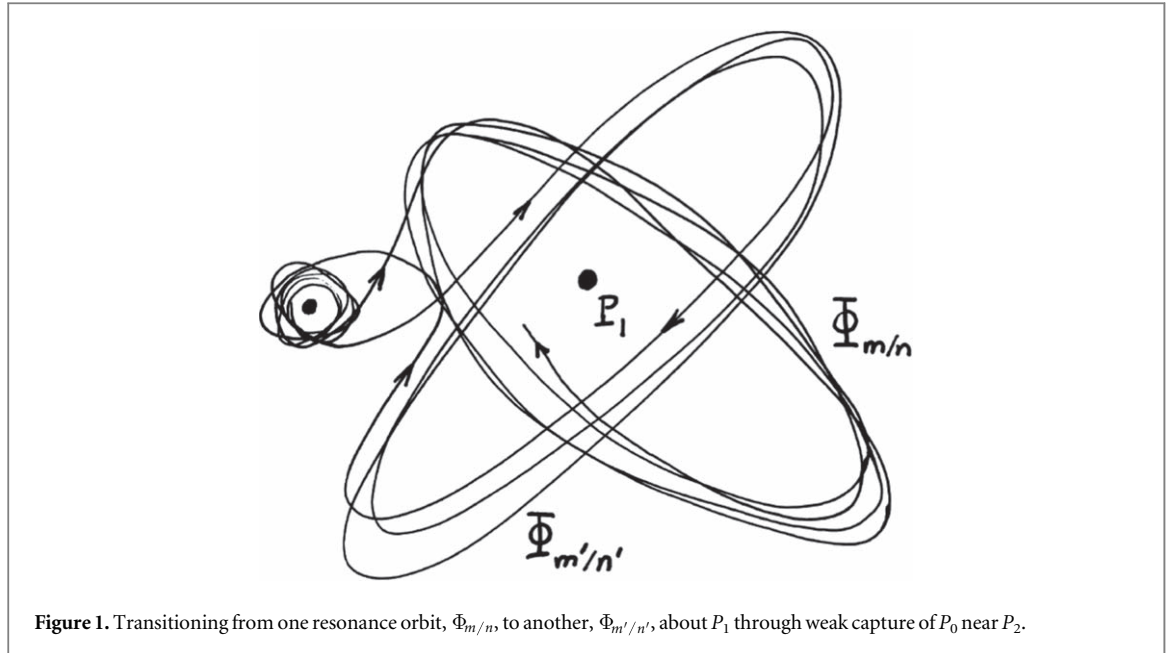


Figure 1. Transitioning from one resonance orbit, $\Phi_{m/n}$, to another, $\Phi_{m'/n'}$, about P_1 through weak capture of P_0 near P_2 .

$$E_1 \equiv E_1(Y, \dot{Y}) = \frac{1}{2}|\dot{Y}|^2 - \frac{G(m_0 + m_1)}{r_1}, \quad (7)$$

where $Y = (Y_1, Y_2)$, $r_1 = |Y|$, are inertial P_1 -centered coordinates. E_1 can be written as $E_1 = -G(m_0 + m_1)/(2a_1)$, [8]. Using Kepler's third law relating the period, T_1 , to a_1 , implies, $E_1 = -A\omega_1^{2/3}$, $A = (1/2)(2\pi G(m_0 + m_1))^{2/3}$. (6) Implies E_1 can be written as,

$$E_1(\Phi_{m/n}(t)) \equiv E_1(m/n) = -[(m/n)\omega]^{2/3}A + \mathcal{O}(\delta), \quad (8)$$

where the remainder is smooth in t . (8) Proves (ii). It is noted that in this case, $E_1 \approx -[(m/n)\omega]^{2/3}A$.

It is noted that E_1 can be written in an equivalent form to (7) by multiplying both sides of (7) by the reduced mass, $\nu = m_0 m_1 (m_0 + m_1)^{-1}$, yielding

$$\tilde{E}_1 \equiv \nu E_1 = \frac{\nu}{2}|\dot{Y}|^2 - \frac{Gm_0 m_1}{r_1}, \quad (9)$$

which implies, $\tilde{E}_1 = -Gm_0 m_1/(2a_1)$. This scaled energy is more convenient to use when the modified Schrödinger equation is considered. To obtain the corresponding two-body differential equations with (9) as an integral, one multiplies the differential equations associated to (7) by ν . The solutions are the same for both sets of differential equations³. Thus, it is seen that $\tilde{E}_1 = \nu E_1 = -\nu A\omega_1^{2/3}$. Setting $\sigma = \nu A$ implies,

$$\tilde{E}_1 = -\sigma\omega_1^{2/3}, \quad (10)$$

$$\sigma = (1/2)(2\pi G)^{2/3}m_0 m_1 (m_0 + m_1)^{-1/3}. \quad (11)$$

ω_1 remains the same since the solutions haven't changed. This defines the function σ that plays a key role in this paper.

2.2. A modified Schrödinger equation: macroscopic scale

Analogy A. It is noted that equation (10) has a form similar to the Planck-Einstein relation for quantum mechanics for the energy, \mathcal{E} , of a photon, $\mathcal{E} = h\lambda$, where λ is the frequency of the photon. σ is analogous to h and $\tilde{\omega}_1^{2/3}$ is analogous to λ . There is another analogy for the case of an electron, P_0 , moving about an atomic nucleus: when P_0 changes from one orbital to another, the energy of the photon absorbed or emitted is given by $\Delta E = h\lambda$, where $\Delta E = E_1 - E_2$, where E_i is the energy of P_0 in the i th orbital, $i = 1, 2$. This process is analogous to a macroscopic particle P_0 changing from from one resonance orbit $\Phi_{m/n}(t)$ in \mathfrak{F} to another, $\Phi_{m'/n'}(t)$, through weak capture and escape, where $\Delta\tilde{E}_1 = \tilde{E}_1(m/n) - \tilde{E}_1(m'/n')$. $\Delta\tilde{E}_1$ is analogous to ΔE .

We consider a modified Schrödinger equation (1). This Schrödinger equation differs from the classical one by replacing \hbar by the function $\sigma = \sigma(m_0, m_1, G)$ and V by a three-body potential \hat{V} derived from the circular restricted three-body problem. The choice of σ is motivated by analogy A. In this modeling, the masses

³ (7) is an integral for $\ddot{Y} = -G(m_0 + m_1)Yr_1^{-3}$, and (9) is an integral for $\nu\ddot{Y} = -Gm_0 m_1 Yr_1^{-3}$.

m_0, m_1, m_2 and distance between them is assumed to not be in the quantum scale. Under this assumption, Ψ does not represent a wave motion and is used to measure the probability of locating P_0 at a distance r_1 from P_1 .

The potential \bar{V} in (1), is derived from the restricted three-body problem modeling for the motion of P_0 . In inertial coordinates, $Y = (Y_1, Y_2)$ centered at P_1, P_2 moves about P_1 on a circular orbit, $\gamma(t)$ of constant radius β and circular frequency $\omega = \sqrt{G(m_1 + m_2)}/\beta, \gamma(t) = \beta(\cos \omega t, \sin \omega t)$. The potential for P_0 is given by

$$\hat{V} = V_1 + V_2, \tag{12}$$

$$V_1 = -\frac{Gm_0m_1}{r}, \quad V_2 = -\frac{Gm_0m_2}{r_2}, \tag{13}$$

where $r = |Y|, r_2 = |Y - \gamma(t)|$. For simplicity of notation, we have replaced the symbol r_1 by r ($r_1 \equiv r$).

We replace V_2 by an approximation given by an averaged value of V_2 over one cycle of $\gamma(t), t \in [0, 2\pi/\omega]$,

$$\bar{V}_2 = -\frac{Gm_0m_2\omega}{2\pi} \int_0^{\frac{2\pi}{\omega}} \frac{dt}{\sqrt{r^2 + \beta^2 - 2\beta(Y_1 \cos \omega t + Y_2 \sin \omega t)}}. \tag{14}$$

It is proven in section 4 that \bar{V}_2 can be reduced to three cases in (48) depending on $r < 0, r = 0, r > 0$, respectively, where the first order term in \bar{V}_2 has a form similar to V_1 .

As an approximation to \hat{V} we use,

$$\bar{V} = V_1 + \bar{V}_2. \tag{15}$$

The modified Schrödinger equation that we consider is given by

$$-\frac{\sigma^2}{2\nu} \nabla^2 \Psi + \bar{V} \Psi = E \Psi, \tag{16}$$

The solution of this modified Schrödinger equation is derived in section 4. The solution is summarized in result B.

Result B. The explicit solution of the modified Schrödinger equation, more generally in a three-dimensional P_1 -centered inertial coordinates, (Y_1, Y_2, Y_3) , (16), is given by,

$$\Psi = R_{\tilde{n},l}(r) Y_{m,l}(\phi, \theta) + \mathcal{O}(m_0 m_2). \tag{17}$$

$\tilde{n} = 0, 1, 2, \dots; l = 0, 1, 2, \dots; -l \leq m_l \leq l, r$ is the distance from P_0 to $P_1, r \geq 0, \phi \in [0, 2\pi]$ is the angle in the Y_1, Y_2 -plane relative to the Y_1 -axis, $\theta \in [0, \pi]$ is the angle relative to the Y_3 -axis. $R_{\tilde{n},l}(r)$ is given by (39) defined using Laguerre polynomials. $Y_{l,m_l} = \Phi_{m_l}(\phi) \Theta_{l,m_l}(\theta)$ are spherical harmonic functions, where $\Phi_{m_l}(\phi), \Theta_{l,m_l}(\theta)$ are given by (35), (37), respectively. $\Theta(\theta)$ is defined by Legendre polynomials.

$|\Psi|^2$ is the probability distribution function of finding P_0 at a location (r, ϕ, θ) . In particular, the radial probability distribution function of finding P_0 at a radial distance r is given by

$$P(r) = R^2(r) r^2 + \mathcal{O}(m_0 m_2), \tag{18}$$

where $R \equiv R_{\tilde{n},l}$.

Ψ exists provided the energy, E , is quantized as,

$$E \equiv \hat{E}_{\tilde{n}} = -\frac{4\sigma}{\tilde{n}^2} + \mathcal{O}(m_0 m_2), \tag{19}$$

where the remainder term is smooth in Y_1, Y_2, Y_3 .

It is noted that the solution of (16) is valid for $\bar{V} = 0$. However, we assume $\bar{V} \neq 0$ to compare with the resonance solutions of three-body problem, where $Y_3 = 0$. All the terms $\mathcal{O}(m_0 m_2)$ are smooth in Y_1, Y_2, Y_3 .

It is assumed that m_0 can be taken sufficiently small, such that for any given small number, $\epsilon_2 > 0$, and for $(Y_1, Y_2, Y_3) \in D, D$ compact, the term $\mathcal{O}(m_0 m_2)$ in (19) satisfies, $|\mathcal{O}(m_0 m_2)| < \epsilon_2$. In this sense, $\hat{E}_{\tilde{n}} \approx -\frac{4\sigma}{\tilde{n}^2}$.

The planar case is now assumed, $Y_3 = 0$, unless otherwise indicated.

Assumptions 1. The use of the approximate symbol for $\hat{E}_{\tilde{n}}$ using $\mathcal{O}(m_0 m_2)$, is different to the one given in definition 1, for ω_1 using $\mathcal{O}(\delta), \delta = m_2/m_1$. In definition 1, $\mathcal{O}(\delta)$ depends on t , and to bound it by a given small number ϵ_1, t varies on a compact set and m_2 is taken sufficiently small. In the second case, $\mathcal{O}(m_0 m_2)$, depends on (Y_1, Y_2) , and to bound it by a small number $\epsilon_2, (Y_1, Y_2)$ varies on a compact set D and m_0 is taken sufficiently small. To satisfy both cases, it is necessary to assume m_0, m_1 are sufficiently small. The use of \approx is taken from context.

2.3. Equivalence of quantized energies with resonance solutions

The quantized values of the energy, $\hat{E}_{\tilde{n}}$, (19), are for the modified Schrödinger equation, (16). These energies are not obtained for the three-body problem, but result from an entirely different modeling. When they are substituted for \hat{E}_1 in the two-body energy relation, (10), for P_0 moving about P_1 , it is calculated in section 4, (53), that they yield rational values for the two-body frequency, ω_1 ,

$$\omega_1|_{\hat{E}_1=\hat{E}_{\tilde{n}}} \equiv \omega_1(\tilde{n}) = \frac{8}{\tilde{n}^3} + \mathcal{O}(m_0 m_2). \quad (20)$$

It is significant that the leading dominant term of $\omega_1(\tilde{n})$ is independent of masses and distances. This implies that to first order the frequencies do not depend on the masses or any other parameters.

Thus, for $\tilde{n} = 1, 2, \dots$, infinitely many frequencies are obtained, $\omega_1(\tilde{n})$. We would like to show that these frequencies correspond to \tilde{n} resonance orbits of \mathfrak{F} for the three-body problem. Hence, we need to compare the frequencies $\omega_1(\tilde{n})$, given by (20), with the frequencies $\omega_1(m/n)$, defined by (6). The following result is obtained,

Result C. The quantized energy values, (19), of the modified Schrödinger equation can be put into a one to one correspondence with a subset, \mathfrak{U} , of the resonance solutions $\Phi_{m/n}(t) \in \mathfrak{F}$ of the circular restricted three-body problem, where

$$\mathfrak{U} = \{\Phi_{m/n}(t) | m = 8, n = \tilde{n}^3, \tilde{n} = 1, 2, \dots\}. \quad (21)$$

This is proven in section 4 by scaling the restricted three-body problem and using the fact that this scaling does not effect the leading order term $\frac{8}{\tilde{n}^3}$ of $\omega_1(\tilde{n})$.

It is noted that $m = 8, n = \tilde{n}^3$ implies that in the time it takes P_0 to make \tilde{n}^3 cycles about P_1 , P_2 makes 8 cycles about P_1 .

As previously noted, the limiting case of $m_2 = 0$ has been excluded in this paper since it is degenerate in the sense that the resonance families of solutions no longer exist. One can make a comparison with quantized two-body elliptic orbits of P_0 about P_1 with the classical Schrödinger equation for $m_2 = 0$ (see [9], page 263), but this case does not yield the transitioning resonance solutions described in this paper.

2.4. Quantum scale

The results presented thus far are for mass values that are not in the quantum-scale. Consider the family, $\mathfrak{U} \subset \mathfrak{F}$, of resonance periodic orbits for P_0 in the three-body problem, whose frequencies, $\omega_1(m, n)$, given by (6), where $m/n \approx 8/\tilde{n}^3$. These frequencies correspond to the quantized energy values, $\hat{E}_{\tilde{n}}$, of the modified Schrödinger equation. When the masses, $m_k, k = 0, 1, 2$, get smaller and smaller, along with the relative distances between the particles, as they approach the quantum-scale, ω_1, ω , increase in value as $r_1^{-1/2}, \beta^{-1/2}$ as $r_1, \beta \rightarrow 0$, respectively. The particles remain gravitationally bound to each other. The mass of P_0 is negligible with respect to that of P_1, P_2 . As the distances decrease, the motions of the particles produces a gravitational field by the circular motion of P_1, P_2 and the resonance motion of P_0 . We refer to this gravitational field as a *resonance gravitational field*.

When the system of three particles reaches the quantum scale they take on a wave-particle duality. The differential equations for the three-body problem are no longer defined. The previous resonance motion of the particles takes on a wave character.

The three-body problem is no longer defined in the quantum scale and therefore result A is no longer valid. However, the modified Schrödinger equation is still well defined. We can now assume the three-dimensional wave solutions. The quantized energy values are still defined, for $\tilde{n} = 1, 2, \dots$. Now, they are identified with pure wave solutions $\Psi(r, \theta)$ given in result B. The values of $\hat{E}_{\tilde{n}}$, can be viewed as taking on wave resonance values. This is summarized in,

Result D. The resonance solutions $\Psi_{m/n}(t) \in \mathfrak{U}$ for P_0 for the three-body problem, which are given by the solutions Ψ , (17), of the modified Schrödinger equation are also given by Ψ when the masses are reduced to the quantum scale. This provides a quantization of the gravitational dynamics of P_1 for the motion of m_0 corresponding to the energies $\hat{E}_{\tilde{n}}$, given by (19).

In the quantum scale, where $\sigma \rightarrow 0$ as $m_0, m_1 \rightarrow 0$, shown in section 4, there is a transition of the resonance solutions into wave solutions, as summarized in result D, using Ψ . However, to make these wave solutions more physically relevant, we would like to have $\sigma(m_0, m_1, G) = \hbar$.

It is shown in section (4), proposition 4.1, that as $m_0, m_1 \rightarrow 0$, there exist mass values where $\sigma(m_0, m_1, G) = \hbar$. These mass values lie on an algebraic curve in (m_0, m_1) -space. For these values of m_0, m_1 , the term $-\frac{\sigma^2}{2\nu} \nabla^2 \Psi$ of the modified Schrödinger equation matches the same term of classical Schrödinger

equation. In this case, only the gravitational potential is present. To make this accurate for atomic interaction, for example, for the motion of an electron about a nucleus of the Hydrogen atom, the gravitational potential needs to be replaced by the Coulomb potential.

If we consider the modified Schrödinger equation, it can be further altered by adding, for example, a Coulomb potential. If the masses are chosen so that $\sigma = \hbar$, then one obtains a classical Newton-Schrödinger equation model [10, 11]. This could also be studied with $\sigma \neq \hbar$.

The wave solutions of the modified Schrödinger equation could be considered in the quantum scale where $\sigma \neq \hbar$. This is not studied in this paper.

3. Weak capture and resonant motions in the three-body problem

In this section we show how to prove result A. The idea of the proof of result A is to utilize the geometry of the phase space about P_1, P_2 , where the motion of P_0 is constrained by Hill's regions. Within the Hill's regions, the dynamics associated to weak capture from near P_2 together with the global properties of the invariant hyperbolic manifolds around P_1 will yield the proof.

The planar circular restricted three-body problem in inertial coordinates is defined in section 2 by (3) for the motion of P_0 . If P_0 moves about P_1 with elliptic initial conditions, and a rotating coordinate system is assumed that rotates with the same constant circular frequency ω between P_1 and P_2 , then the motion is understood by the Kolmogorov-Arnold-Moser (KAM) theorem [1, 8]. It says that nearly all initial elliptic initial conditions of P_0 with respect to P_1 give rise to quasi-periodic motion, of the two frequencies, ω_1, ω , where ω_1 is the frequency of the elliptic motion of P_0 about P_1 , provided they satisfy the condition that ω_1/ω is sufficiently non-rational. For the relatively small set of motions of P_0 where ω_1/ω is sufficiently close to a rational number, the motion is chaotic. It is also necessary to assume that $\mu = m_2/(m_1 + m_2)$ is sufficiently small.

The planar modeling is assumed without loss of generality. This follows since the resonance orbits we will be considering for P_0 moving about P_1 are approximately two-body in nature. This implies approximate planar motion. These same orbits result from weak capture conditions and escape, which imply that the plane of motion of P_0 about P_1 will approximately be the same plane of motion as that of P_2 about P_1 . Thus, co-planar modeling assumed in the restricted three-body problem is a reasonable assumption.

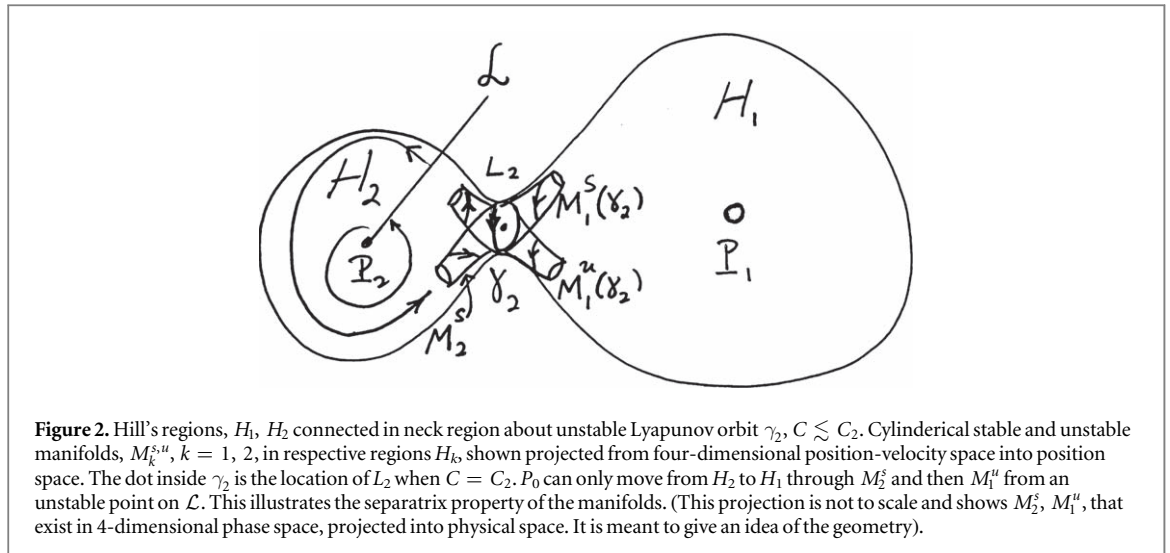
Whereas the motion of P_0 about P_1 is well understood by the KAM theorem for small m_2 , the general motion of P_0 about P_2 is not well understood since it's considerably more unstable. The instability arises due to the fact that m_2 is much smaller than m_1 , and the KAM theorem cannot be easily applied unless P_0 moves infinitely close to P_2 [12]. This implies that if P_0 starts with an initial two-body elliptic state with respect to P_2 , its trajectory is substantially perturbed by the gravitational effect of P_1 . The resulting motion of P_0 about P_2 is unstable and generally rapidly deviates from the initial elliptic state. Numerical simulations show the motion to be chaotic in nature. Results described in this section provide a way to better understand motion about P_2 .

The notion of weak capture (defined in section 2) of P_0 about P_2 is useful in trying to understand the motion of P_0 about P_2 with initial elliptic conditions. The idea is to numerically propagate trajectories of the three-body problem with initial conditions that have negative energy, $E_2 < 0$, with respect to P_2 , and measure how they cycle about P_2 , described in more detail later in this section. Generally, if P_0 performs k complete cycles about P_2 , relative to a reference line emanating from P_2 , without cycling about P_1 , then the motion of P_2 is called 'stable', provided it returns to the line with $E_2 < 0$, while if does not return to the line after $(k - 1)$ complete cycles, and cycles about P_1 , the motion is called 'unstable'. It is also called unstable if P_0 does return to the line, but where $E_2 > 0$. (see figure 4) The line represents a two-dimensional surface of section in the four-dimensional phase space, \mathbb{R}^4 . The set of all stable points about P_2 defines the ' k th stable set', W_k^s , and the set of all unstable points is called the ' k th unstable set', W_k^u . Points that lie on the boundary between W_k^s and W_k^u define a set, \mathcal{W}_k , called the ' k th weak stability boundary'. The boundary points are determined algorithmically, by iterating between stable and unstable points [13].

Points that belong to W_k^u are in weak capture with respect to P_2 since they start with $E_2 < 0$, which lead to escape with $E_2 > 0$ (proposition 3.1). However, this may not be the case for points in W_k^s since after they cycle about P_2 k times, it is possible they can remain moving about P_2 for all future time and E_2 will be negative each time P_0 intersects the line.

\mathcal{W}_k was first defined in [14], for the case $k = 1$. This set has proved to have important applications in astrodynamics to enable spacecraft to transfer to the Moon and automatically go into weak capture about the Moon, that requires no fuel for capture. This was a substantial improvement to the Hohmann transfer, which requires substantial fuel for capture [8, 15]⁴. It also has applications in astrophysics on the Lithopanspermia

⁴ It was first used operationally in 1991 to rescue a Japanese lunar mission by providing a new type of transfer from the Earth to the Moon used by its spacecraft, *Hiten*.



Hypothesis [16]. The weak stability boundary was generalized to k -cycles, $k > 1$, with new details about its geometric structure in [17]. [13] makes an equivalence of \mathcal{W}_k with the stable manifolds of the Lyapunov orbits associated to collinear Lagrange points.

$W_k^s, W_k^u, \mathcal{W}_k$ are defined more precisely: we transform from $X = (X_1, X_2)$ defined in (3) to a rotating coordinate system, $x = (x_1, x_2)$, that rotates with frequency ω , so that in this system, P_1, P_2 are fixed on the x_1 -axis. Scaling $m_1 = 1 - \mu, m_2 = \mu, \mu > 0, G = 1, \beta = 1, \omega = 1$, as mentioned in section 2, we place P_1 at $x = (\mu, 0)$ and P_2 at $(-1 + \mu, 0)$. (3) becomes,

$$\ddot{x} + 2(-\dot{x}_2, \dot{x}_1) = \tilde{\Omega}_x, \tag{22}$$

$\tilde{\Omega} = (1/2)|x|^2 + (1 - \mu)r_1^{-1} + \mu r_2^{-1} + (1/2)\mu(1 - \mu)$, $r_1 = |x - (\mu, 0)|, r_2 = |x - (-1 + \mu, 0)|$. The Jacobi integral function, $J(x, \dot{x})$ for this system is given by

$$J = 2\tilde{\Omega} - |\dot{x}|^2. \tag{23}$$

The differential equations have 5 well known equilibrium points, $L_i, i = 1, 2, 3, 4, 5$, where L_1, L_2, L_3 are the collinear Lagrange points, and L_4, L_5 are equilateral points. We assume the convention that L_2 lies between P_1, P_2 . $J|_{L_i} = C_i$, where $3 = C_4 = C_5 < C_3 < C_1 < C_2$. The collinear points are all local saddle-center points with eigenvalues, $\pm\alpha$ and $\pm i\beta, \alpha > 0, \beta > 0, i^2 = -1$. The equilateral points L_4, L_5 are locally elliptic points. We will focus on L_1, L_2 in our analysis. As is described in [8, 18], the distance of L_1, L_2 to $P_2, r_{L_j}, j = 1, 2$, is $r_{L_j} = \mathcal{O}(\mu^{1/3})$. $C_j = 3 + |\mathcal{O}(\mu^{2/3})| \gtrsim 3$ for $\mu \gtrsim 0$.

Projecting the three-dimensional Jacobi surface $J^{-1}(C)$ into physical (x_1, x_2) -space, yields the Hill's regions, where P_0 is constrained to move. (see [8], figure 3.6) For C slightly greater than $C_2, C \gtrsim C_2$, the Hill's regions about P_1, P_2 , labeled H_1, H_2 , respectively, are not connected, so that P_0 cannot pass from one region to another. There is also a third Hill's region, H_3 that surrounds both P_1, P_2 disconnected from H_1, H_2 , where P_0 can move about both primaries. When $C = C_2, H_1, H_2$ are connected at the single Lagrange point L_2 and P_0 still cannot pass between the primaries. When $C \lesssim C_2$, a small opening occurs between P_1, P_2 near the L_2 location, we refer to as a neck region, N_2 , first discussed in [19]. When C decreases further, $C \lesssim C_1$, another opening occurs near L_1 and forms another neck region, N_1 , that connects H_2 with the outer Hill's region, H_3 .

A retrograde unstable hyperbolic periodic orbit is contained in N_2 , we label γ_2 . γ_2 has local stable and unstable two-dimensional manifolds $M_j^s(\gamma_2), M_j^u(\gamma_2), j = 1, 2$, which extend from N_2 into H_j . These manifolds are topologically equivalent to two-dimensional cylinders. It is shown in [19] that orbits can only pass from H_2 to H_1 , or from H_1 to H_2 , by passing within the three-dimensional region contained inside $M_j^s(\gamma_2), M_j^u(\gamma_2)$, which are called transit orbits. For example, to pass from H_2 to H_1, P_0 must pass into the three-dimensional region inside $M_2^s(\gamma_2) \subset H_2$ and out from the region inside $M_1^u(\gamma_2) \subset H_1$ (see figure 2) (see also [8], figure 3.9). N_2 is bounded on either side of P_2 by vertical lines l_R, l_L , that cut the x_1 -axis, to the right and left of P_2 , respectively. On the Jacobi surface, $\{J = C\}, J^{-1}(N_2)$ is a set with topological two-dimensional spheres as boundaries, S_R^2, S_L^2 corresponding to the lift of l_R, l_L , respectively, onto $\{J = C\}$. When a transit orbit passes from H_2 to H_1 , then on the Jacobi surface, P_0 passes from S_L^2 to S_R^2 . The bounding spheres separate H_1, H_2 from N_2 .

For $C \lesssim C_1, N_1$ contains the Lyapunov orbit γ_1 . Manifolds, $M_j^s(\gamma_2), M_j^u(\gamma_2), j = 2, 3$, are similarly obtained where transit orbits can pass between H_2 and H_3 , passing through the respective bounding spheres. The geometry in this case is shown in figure 3).

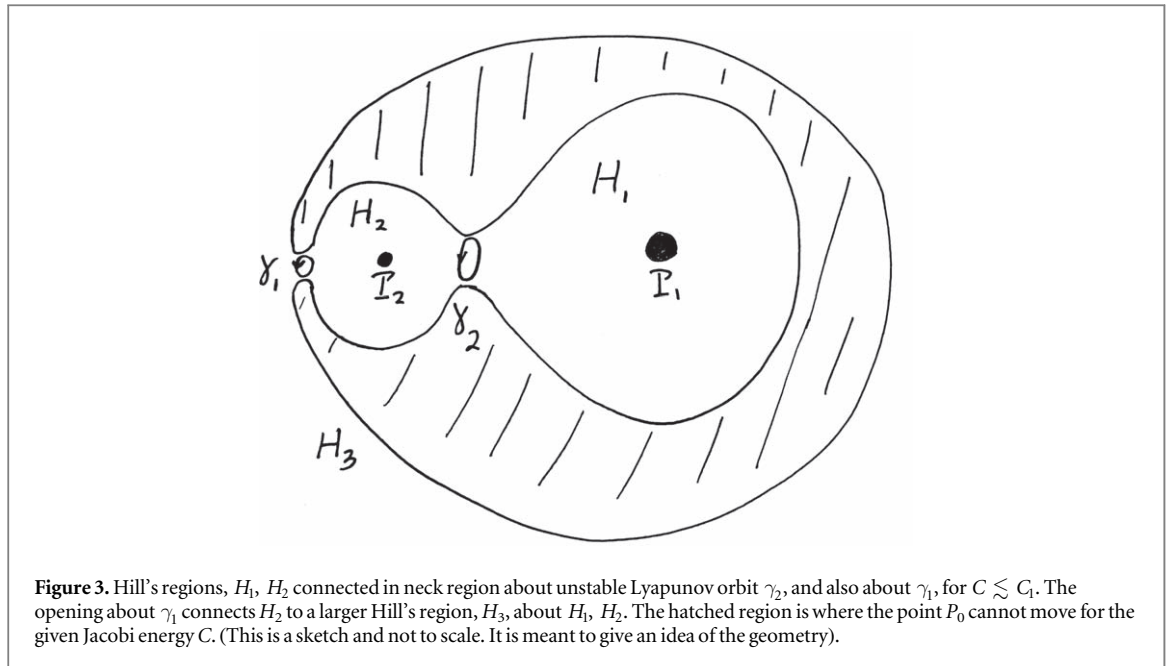


Figure 3. Hill's regions, H_1 , H_2 connected in neck region about unstable Lyapunov orbit γ_2 , and also about γ_1 , for $C \lesssim C_1$. The opening about γ_1 connects H_2 to a larger Hill's region, H_3 , about H_1 , H_2 . The hatched region is where the point P_0 cannot move for the given Jacobi energy C . (This is a sketch and not to scale. It is meant to give an idea of the geometry).

It is noted that in center of mass, rotating coordinates, (x_1, x_2) , (5) becomes,

$$E_{2R} = \frac{1}{2}|\dot{x}|^2 + \frac{1}{2}|x|^2 - \omega(\dot{x}_1x_2 - \dot{x}_2x_1) - \frac{G(m_0 + m_2)}{r_2}, \tag{24}$$

with $\omega = 1$, $m_0 = 0$, $m_2 = \mu$, $G = 1$.

Finally, a translation, $z_1 = x_1 - (-1 + \mu)$, $z_2 = x_2$, is made to a P_2 -centered coordinate system, (z_1, z_2) , where P_1 is at $(1, 0)$, and $r_2 = |z|$. For notation, we set $r \equiv r_2$. We refer to E_{2R} in center of mass rotating coordinates (x_1, x_2) and also in P_2 -centered rotating coordinates (z_1, z_2) , where E_{2R} is a different expression from (24).

The line \mathcal{L} emanates from P_2 and makes an angle $\theta_2 \in [0, 2\pi]$ with respect to the z_1 -axis. Trajectories of P_0 are propagated from \mathcal{L} such that at each point on \mathcal{L} at a distance $r > 0$, the eccentricity, e_2 , is kept fixed to a value, $e_2 \in [0, 1)$, by adjusting the velocity magnitude, whose initial direction is perpendicular to \mathcal{L} . Also, the velocity direction is assumed to be clockwise (similar results are obtained for counter clockwise propagation). The initial points of propagation on \mathcal{L} are periapsis points of an osculating ellipse of velocity $v_p = \sqrt{G(m_0 + m_2)(1 + e_2)/r} - \omega r$, $\omega = 1$, $m_0 = 0$, $m_2 = \mu$. It is noted that \mathcal{L} makes a two-dimensional surface of section, defined in polar coordinates, $S_{\theta_2^0} = \{(r_2, \theta_2, \dot{r}_2, \dot{\theta}_2 | \theta_2 = \theta_2^0, \dot{\theta}_2 > 0\}$. It is also noted that as r changes on \mathcal{L} , the Jacobi energy also changes. This implies that W_k^u , W_k^s , \mathcal{W} do not lie on a fixed Jacobi surface. Also the Hill's regions vary within these sets.

As is described in [13, 17], a sequence of consecutive open intervals, I_j^k , are obtained along \mathcal{L} , for a fixed θ_2, e_2 , that alternate between stable and unstable points, for k cycles. That is, $I_1^k = \{r_0^k < r < r_1^k\}$, $r_0^k = 0$, are stable points, $I_2^k = \{r_1^k < r < r_2^k\}$ are unstable points, etc (see figure 4) There are $N_k(\theta_2, e_2)$ stable sets, and unstable sets, for an integer $N_k \geq 1$. The boundary points r_j^k , $j = 1, 2, \dots, N_k(\theta_2, e_2)$, represent the transition between stable and unstable points relative to k cycles, where the k th unstable points lead to stable motion for $k - 1$ cycles and are unstable on the k th cycle. The k th stable set for a given value of θ_2, e_2 is given by,

$$W_k^s(\theta_2, e_2) = \bigcup_{j=0}^{N_k(\theta_2, e_2)} (r_{2j}^k, r_{2j+1}^k). \tag{25}$$

This is a slice of the entire stable set, W_k^s , by varying θ_2, e_2 , given by

$$W_k^s = \bigcup_{\theta \in [0, 2\pi], e \in [0, 1)} W_k^s(\theta_2, e_2). \tag{26}$$

We define $\mathcal{W}_k = \partial W_k^s$. \mathcal{W}_k has a Cantor-like structure as is described in [13]. The numerical estimation of W_k^s, \mathcal{W}_k is given in [13, 17, 20], for different values of k, μ, θ_2, e_2 . The motion of P_0 is seen to be unstable and sensitive for initial conditions near \mathcal{W}_k . It is remarked that due to limitations of computer processing time, k is not taken too large.

A main result of [13], is that \mathcal{W}_k about P_2 is equivalent to the set of global stable manifolds, $M_2^s(\gamma_1) \cup M_2^s(\gamma_2)$, to the Lyapunov orbits, γ_1, γ_2 , respectively, about the collinear Lagrange points, L_1, L_2 , on

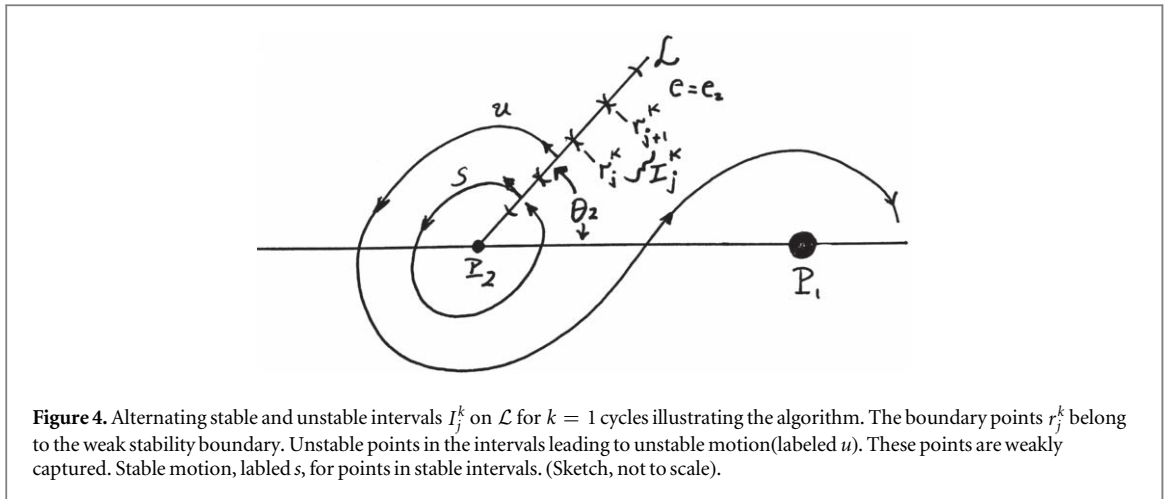


Figure 4. Alternating stable and unstable intervals I_j^k on \mathcal{L} for $k = 1$ cycles illustrating the algorithm. The boundary points r_j^k belong to the weak stability boundary. Unstable points in the intervals leading to unstable motion (labeled u). These points are weakly captured. Stable motion, labeled s , for points in stable intervals. (Sketch, not to scale).

either side of P_2 for $C \lesssim C_1$ and μ sufficiently small, in H_2 . Similarly, one could restrict $C \lesssim C_2$ and have equivalence to only the global manifold $M_2^s(\gamma_2)$ in H_2 . This is demonstrated numerically by examining the intersections of $M_2^s(\gamma_1)$, $M_2^s(\gamma_2)$ on surfaces of section $S_{\theta_2^0}$ satisfying $\dot{r} = 0$, $E_2 < 0$ for μ sufficiently small, and varying $0 \leq \theta_2^0 \leq 2\pi$. It is shown in [13] that a very small set of points exist on \mathcal{W}_k that do not satisfy this equivalence. These points are not considered⁵.

The reason this equivalence is true is due to the separatrix property of the manifolds (see [13, 19]). Assume $C \lesssim C_2$. The separatrix property means that if a trajectory point is inside of the region bounded by $M_2^s(\gamma_2)$ on \mathcal{L} , it will wind about P_2 staying inside the region contained by $M_2^s(\gamma_2)$ as $M_2^s(\gamma_2)$ winds about P_2 . P_0 can't go outside this manifold region. Eventually, $M_2^s(\gamma_2)$ will go to γ_2 , and P_0 will pass through N_2 into H_1 as a transit orbit, after it makes $k - 1$ complete cycles, before completing the k th cycle. This corresponds to an unstable point on the set W_k^u . If a trajectory point is outside $M_2^s(\gamma_2)$ on \mathcal{L} , P_0 will remain in H_2 , making k complete cycles about P_2 near the outside of $M_2^s(\gamma_2)$, but it can't escape to H_1 . Thus, $M_2^s(\gamma_2)$ itself is equivalent to \mathcal{W}_k . That is, $M_2^s(\gamma_2)$ separates between stable and unstable motion.

The intersections of $M_2^s(\gamma_2)$ on \mathcal{L} in physical space as it cycles around P_2 give rise to the alternating intervals between stable and unstable motion, $\{I_1^k, I_2^k, \dots\}$, where there are $N_k(\theta_2, e_2)$ such intervals. Points inside $M_2^s(\gamma_2)$ on \mathcal{L} correspond to points in the set W_k^u , and points outside of $M_2^s(\gamma_2)$ on \mathcal{L} , and close to it, correspond to points of the set W_k^s .

The relationship between the manifolds and W_k^s , W_k^u is shown in figure 5.

It can be shown that if $M_2^s(\gamma_2)$ has transverse intersections, which is numerically demonstrated, where the manifold tube breaks, the separatrix property is still satisfied even though a section through the tube no longer gives a circle, but rather parts of broken up circles.

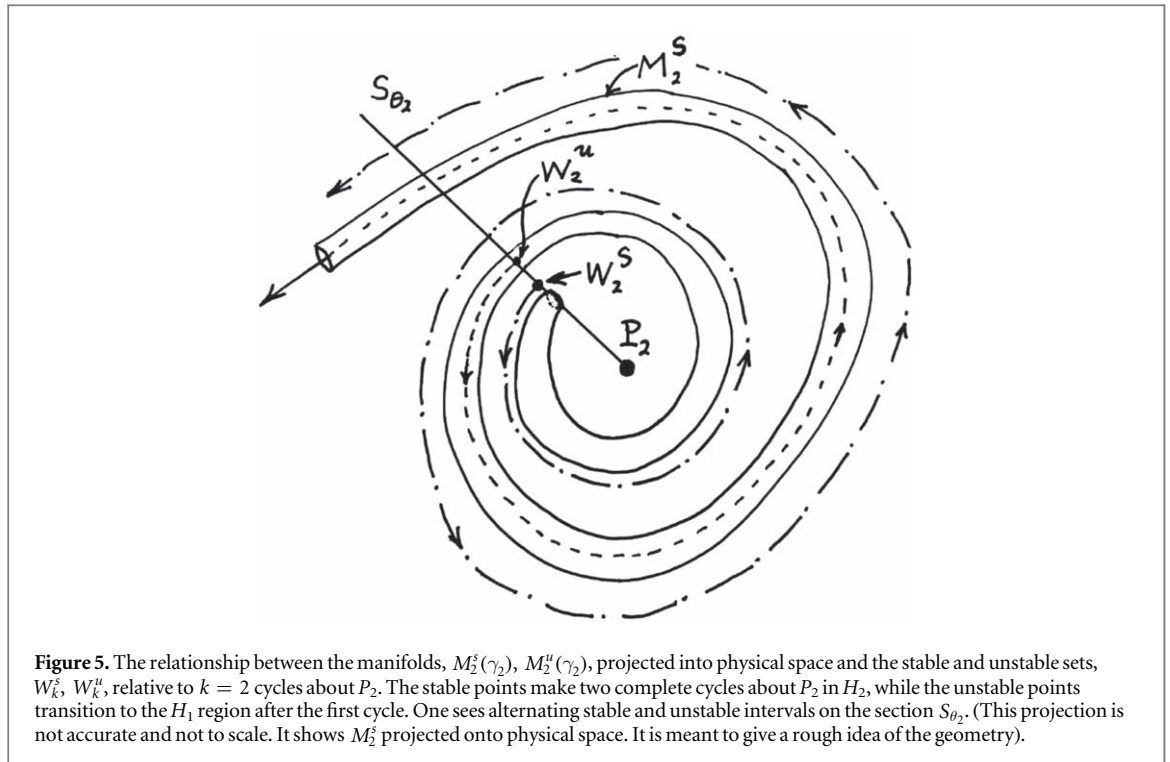
Numerical simulations in [13, 18], indicate for $C \lesssim C_1$, that $M_2^s(\gamma_1)$ can intersect $M_2^u(\gamma_2)$ transversally, giving rise to a complex network of invariant manifolds about P_2 , and for $C \lesssim C_2$, $M_2^u(\gamma_2)$ can intersect $M_2^s(\gamma_2)$ transversally, for a set of μ and C . This supports the fact that the motion near \mathcal{W}_k is sensitive.

Let $\zeta(t) = (z_1(t), z_2(t), \dot{z}_1(t), \dot{z}_2(t)) \in \mathbb{R}^4$ be the trajectory of P_0 in rotating P_2 -centered coordinates, and $z(t) = (z_1(t), z_2(t)) \in \mathbb{R}^2$ the trajectory of P_0 in physical coordinates. Similarly, in inertial P_2 centered coordinates, we define, $\mathcal{Z}(t) = (Z_1(t), Z_2(t), \dot{Z}_1(t), \dot{Z}_2(t))$, and $Z(t) = (Z_1(t), Z_2(t))$. We will use inertial and rotating coordinates to describe the motion of P_0 .

The following result, referenced previously, is proven,

Proposition 3.1 ($P_0 \in W_k^u$ implies P_0 is weakly captured by P_2). Assume $P_0 \in W_k^u$ at time $t = t_0$, which implies $E_2(t_0) < 0$. There are two possibilities: (i.) P_0 cycles about P_2 $k - 1$ times, then moves to cycle about P_1 without cycling about P_2 . This implies that P_0 weakly escapes P_2 . That is, there exists a time $t^* > t_0$, after the $(k - 1)$ st cycle where $E_2(t^*) = 0$, $E_2 \gtrsim 0$ for $t \gtrsim t^*$, and $E_2(t) < 0$ for $t_0 \leq t < t^*$, (ii.) P_0 does k complete cycles about P_2 , where on the k th cycle P_0 returns to \mathcal{L} with $E_2 > 0$. (It is assumed the set of collision orbits to P_1 and P_2 , Γ , are excluded which are a set of measure 0.)

⁵ It is noted that the proof of equivalence of \mathcal{W}_k with the global stable manifolds to L_1 , L_2 in [13] is numerically supported and based on rigorous analytical estimates. Thus, the proof is rigorous in that sense. This is also true of the structure of \mathcal{W}_k obtained in [17]. A purely analytic proof for the global manifold structure about P_2 and \mathcal{W}_k is not available at this time. However, in the case of motion about P_1 , the analogous structure of \mathcal{W}_k is analytically proven [21].



Proof of proposition 3.1–(i). This is shown to be true by noting that when P_0 does a cycle about P_1 , it will cross the x_1 -axis, where $r_2 > 1 + c$, $c > 0$. (24) implies that $E_{2R} = (1/2)\dot{x}_1^2 + (1/2)\mu^2 + \dot{x}_2(1 + c) - \mu(1 + c)^{-1}$, where $\dot{x}_2 > 0$, $\mu \ll 1$. This implies there exists a time t^{**} where $E_{2R} > 0$. Since $E_{2R} < 0$ at $t = t_0$, then there exists a time $t_0 < t^* < t^{**}$ where $E_{2R} = 0$ and $E_2 \gtrsim 0$ for $t \gtrsim t^*$. (ii.) This yields weak capture since $E_2 < 0$ for $t = t_0$ and E_2 becomes positive. Thus, there exists a time t^* where $E_2(t^*) = 0$, then becomes slightly positive.

Global trajectory after weak capture

We rigorously prove result A, that after weak capture with respect to P_2 , P_0 can move onto a resonance orbit about P_1 in resonance with P_2 , and then return to weak capture. This is done by a series of Propositions.

The following sets are defined for trajectories for P_0 starting in weak capture at $t = t_0$ that go to weak escape at a time $t_1 > t_0$.

Assumptions A.

Type I = $\{ \zeta = (z, \dot{z})$ at t_0 is on or near W_k^u ($E_2 < 0$, $\dot{r} = 0$ or $|\dot{r}| \gtrsim 0$, resp.) }

Type II = $\{ \zeta(t_0) = (z(t_0), \dot{z}(t_0))$ is not near W_k^u , where $|\dot{r}(t_0)|$ is not near 0 and $E_2(t_0) < 0$ }

Type IIa = $\{ \zeta(t_0)$ is a Type II point where $\zeta(t)$ goes to weak escape at $t_1 > t_0$ with $|\dot{r}(t_1)|$ not near 0 } (i.e. there is no cycling about P_2 .)

Type IIb = $\{ \zeta(t_0)$ is a Type II point where there exists a time $\hat{t} > t_0$, such that $\zeta(\hat{t})$ on or near $W_{k'}^u$, for some integer $k' \geq 1$ }

Case A = $\{ P_0$ cycles about P_2 ($k - 1$) times, then moves to cycle about P_1 }

Case B = $\{ P_0$ does not cycle about P_1 after ($k - 1$) st cycle. Instead, on k -th cycle about P_2 , P_0 returns to \mathcal{L} with $E_2 > 0$ }

$\Gamma = \{ P_0$ goes to collision with P_1 or P_2 for $t > t_0$ }

Result A is stated more precisely as,

Theorem A. Assume P_0 is weakly captured at a distance r from P_2 at $t = t_0$. Assume the weak capture point, $\zeta(t_0)$ is of Type I, Type IIb, Case A, which are numerically observed to be generic [13], and assume the following sets are ruled out: Type IIa, Case B, Gamma (numerically observed to be small [13]). Assume also that $C \lesssim C_2, \mu$ sufficiently small.

Then P_0 will escape P_2 through N_2 by passing within the region contained within $M_2^s(\gamma_2) \subset H_2$, and moving into the H_1 through the region within $M_1^u(\gamma_2)$. This escape is approximately parabolic since $E_2 \approx 0$ on $S_R^2 \subset H_1$. (Parabolic escape is when there exists a time $t > t_0$ where $E_2 = 0$.) $\zeta(t)$ evolves into an approximate resonance orbit about P_1 with an apoapsis near S_R^2 of N_2 , performing several cycles about P_1 , then returns to S_R^2 passing through N_2 within the region contained within $M_1^s(\gamma_2)$ and exiting N_2 through the interior of $M_2^u(\gamma_2)$ and moving onto weak capture about P_2 . The process repeats unless P_0 moves on any of the sets: Type IIa, Case B, Γ , or P_0 escapes the P_1, P_2 -system.

If $C \lesssim C_1$, then P_0 can parabolically escape P_2 through S_R^2 of N_2 , as previously described obtaining a sequence of resonance orbits in H_1 , or it can parabolically escape P_2 through $S_L^2 = \partial N_1$ into H_3 , by passing through the region within $M_2^s(\gamma_1)$ and exiting from the region within $M_3^u(\gamma_1)$, and form a larger resonance orbit about P_1 with a periapsis near S_L^2 in H_3 , which eventually returns to weak capture about P_2 through N_1 , reversing the previous pathway. This process terminates if P_0 moves on any of the sets Type IIa, Case B, Γ or escapes the P_1, P_2 system.

This yields a sequence of approximate resonance orbits depending on the choice of the weak capture initial condition. The set of all such resonance orbits form the family, \mathfrak{F} . The frequencies of these orbits satisfy (6) of lemma A.

Proposition 3.2 (Capture by P_2 implies weak capture). Let P_0 be captured with respect to P_2 at a distance r from P_2 at a time t_0 , where $E_2(\mathcal{Z}(t_0)) = E_{2R}(\zeta(t_0)) < 0$. Then, P_0 is weakly captured at t_0 . That is, P_0 moves to weak escape at a time $t = t^* > t_0$, where $E_2(\mathcal{Z}(t^*)) = 0$, $E_2(\mathcal{Z}(t)) \gtrsim 0$, $t \gtrsim t^*$. (It is assumed Type IIa, Case B, Γ points are excluded.)

Proof of proposition 3.2. We distinguish several types of weak capture points.

Type I is where P_0 is on or near W_k^u at $t = t_0$. In this case, P_0 is at a distance r from P_2 where $\dot{r} = 0$ or $|\dot{r}| \gtrsim 0$, where we have made use of the fact W_k^u is open, so that $e_2 < 1$ and $E_2(t_0) < 0$. Thus, P_0 is captured at $t = t_0$. For $t > t_0$, the proof follows by proposition 3.1.

Type II is where P_0 is not near W_k^u since $|\dot{r}|$ is not near 0 at $t = t_0$. There are two types. Type IIa is where P_0 starts at $t = t_0$ with E_2 and then to weak escape, with no cycling, by definition. If P_0 starts on a Type IIb point for $t = t_0$, then for $t > t_0$ there will be a time $\hat{t} > t_0$ where $\dot{r} = 0$ or $|\dot{r}| \gtrsim 0$. In that case, P_0 is on or near $W_{k'}^u$ at $t = \hat{t}$, for some $k' \geq 1$. This yields a Type I point, that implies weak capture.

In all these cases, P_0 moves to weak escape at a time $t = t^* > t_0$, where $E_{2R}(\zeta(t^*)) = 0$, $E_{2R}(\zeta(t)) \gtrsim 0$, $t \gtrsim t^*$. This proves proposition 3.2.

As in [13], we exclude Type IIa points as they are not generic. Points on Γ are a set of measure 0 and can be omitted. Case B points are non-generic and excluded.

We now determine what kind of motion P_0 has about P_2 for times up to weak escape at t^* . Consider the trajectory of P_0 as it undergoes counterclockwise cycling about P_2 after leaving points on or near W_k^u on a line \mathcal{L} in both Types I, IIb. (similar results are obtained for clockwise cycling) As P_0 performs $k - 1$ cycles, it either has weak escape prior to completing the k th cycle, where $E_2 = 0$, and then when it intersects \mathcal{L} , $E_2 > 0$, we call Case B, or it moves to cycle P_1 after the $(k - 1)$ st cycle where it was shown in proposition 3.1 that P_0 achieves weak escape, we refer to as Case A.

Proposition 3.3 (P_0 escapes from P_2 through the N_1, N_2 regions). Assume $P_0 \in W_k^u$ at $t=0$, $C \lesssim C_2$, assuming Case A, and excluding Case B. Then after $(k - 1)$ -cycles about P_2 , P_0 moves away from P_2 , passing through the interior region of $M_2^s(\gamma_2)$ into N_2 , between H_2 and H_1 , through the interior of $M_1^u(\gamma_2)$, into H_1 where it starts to cycle P_1 . When P_0 is within N_2 , $E_2 \lesssim 0$. If $C \lesssim C_1$, then after $(k - 1)$ -cycles about P_2 , P_0 moves away from P_2 , passing through the interior of $M_2^s(\gamma_2)$ into N_2 between H_2 and H_1 , and out into H_1 as before, or P_0 passes through the interior of $M_2^s(\gamma_1)$ into N_1 between H_2 and H_3 , and out into H_3 through the interior of $M_3^u(\gamma_1)$. When P_0 is within N_1 , $E_2 \lesssim 0$.

Proof of proposition 3.3. Case A is considered with $C \lesssim C_2$. P_0 starts on \mathcal{L} at $t = t_0$ with $E_2 < 0$, $\dot{r} = 0$. It cycles about P_2 , completes the $(k - 1)$ st cycle, then moves to H_1 where it starts to cycle about P_1 , where $\dot{\theta}_1 > 0$, for $0 \leq \theta_1 \leq 2\pi$ (see [8]). By the separatrix property P_0 is within the interior region contained by $M_2^s(\theta_2)$ on \mathcal{L} at $t = t_0$ and it must pass from P_2 , through N_2 , where it is a transit orbit [13]. When P_0 passes through N_2 it must pass inside the region bounded by $M_2^s(\gamma_2)$, and emerge from N_2 inside the region bounded by $M_1^u(\gamma_2)$ at S_R^2 , where it will begin to cycle about P_1 . For μ sufficiently small, the width of N_2 is near 0, and geometrically this implies the velocity of P_0 with respect to P_2 is near 0 since it passes close to L_2 in phase space.

When $P_0 \in S_R^2$ in H_1 , the distance from P_0 to P_2 can be estimated. The value of $C \lesssim C_2$, and $C_2 = 3 + (\mu/3)^{2/3} + \mathcal{O}(\mu/3)$. P_2 is near L_2 . It directly follows that $r \equiv r_2 = (\mu/3)^{1/3} + \mathcal{O}((\mu/3)^{2/3})$. (This implies, $r_1 = 1 - |\mathcal{O}((\mu/3)^{1/3})| \lesssim 1$ since P_0 is slightly to the right of L_2 at S_R^2 .)

The estimate of r_2 implies that for μ sufficiently small $r_2 \approx \mu/3$. Also, at L_2 , $\dot{x} = 0$. Thus, equation (24) implies

$$E_{2R} = (-3^{1/3} + (1/2)3^{-2/3})\mu^{-2/3} + \mathcal{O}(\mu^b) \lesssim 0, \tag{27}$$

$b > 2/3$.

Case A is considered with $C \lesssim C_1$. (As r increases along \mathcal{L} , keeping a constant eccentricity, C will decrease and move slightly below the other value, C_1 for L_1 , 180 degrees away from L_2 on the anti- P_1 side of P_2 , $C \lesssim C_1$.) As t increases from t_0 , by the separatrix property, P_0 has two possibilities: (i) P_0 can pass through the region bounded by $M_2^s(\gamma_1)$, through N_1 and exiting within the region bounded by $M_3^u(\gamma_1)$ into H_3 intersecting $S_L^2 = \partial N_1$ at a time t_1 . It can then start to cycle about P_1 in H_3 for $t > t_1$, where $\theta_{eta_1} > 0$. This implies unstable motion occurs, where after $(k - 1)$ -cycles about P_2 , P_0 starts to cycle about P_1 in the H_3 region. It is similarly verified that (27) is satisfied on S_L^2 at $t = t_1$. This is different from when P_0 cycles about P_1 after $(k - 1)$ -cycles as it emerges from N_2 into the H_1 region. However, in both cases, as seen, $E_2 \lesssim 0$ in the neck region bounding spheres. (ii) P_0 passes through N_2 into H_1 . This yields the same results as in Case A. (It is verified that $C \lesssim C_1$ is sufficient to yield the same estimates in this proof for E_{2R} as obtained for $C \lesssim C_2$.)

In summary, given $P_0 \in W_k^u$ at time $t = t_0$ there exists a time $t_1 > t_0$ where $E_2 \lesssim 0$ which occurs at $S_R^2 \subset H_1$ for $C \lesssim C_2$, and for $C \lesssim C_1$, $E_2 \lesssim 0$ on $S_L^2 \subset H_3$, or on $S_R^2 \subset H_1$. Thus, in both cases, approximate parabolic escape occurs.

In the next step, we see what happens as P_0 starts to move about P_1 after leaving $S_R^2 = \partial N_2$ in H_1 , or $S_L^2 = \partial N_1$ in H_3 , through $M_1^u(\gamma_2)$, or $M_3^u(\gamma_1)$, respectively.

Proposition 3.4 (P_0 leaves S_R^2 (S_L^2), moves in approximate resonance orbit about P_1 , returns to S_R^2 (S_L^2) and then to weak capture by P_2). Assume $P_0 \in S_R^2 \subset H_1$ at $t = t_1$. P_0 moves from S_R^2 for $t > t_1$ into an approximate resonance orbit about P_1 . After j cycles, $j \geq 1$, P_0 returns to S_R^2 where $E_2 \lesssim 0$. It then moves through N_2 to weak capture by P_2 .

(Similarly, assuming $P_0 \in S_L^2 \subset H_3$ at $t = t_1$, P_0 moves from S_L^2 for $t > t_1$ into an approximate resonance orbit about P_1 in the outer Hills region H_3 . After j cycles, $j \geq 1$, about P_1 , P_0 returns S_L^2 where it then moves through N_1 to weak capture by P_2 .)

Proof of proposition 3.4. The case of $P_0 \in S_R^2 \subset H_1$ is considered first, where $t = t_1$, $C \lesssim C_2$. [21] is referenced since it determines the set \mathcal{W}_k about the larger primary P_1 analytically.

When $P_0 \in S_R^2$ for $t = t_1$, this implies it lies in the three-dimensional region bounded by M_1^u . Moreover, for $t > t_1$, due to the separatrix property, P_0 stays within this region inside M_1^u for all time moving forward [21]. This manifold stays within a bounded region, \mathfrak{M}_1 , bounded by the following: S_R^2 , the boundary of H_1 (a zero velocity curve), and a two-dimensional McGehee torus, T_M , about P_1 [18, 21]⁶. The width of \mathfrak{M}_1 is $\mathcal{O}(\mu^{1/3})$.

There are two cases. The first is where M_1^u is a homoclinic two-dimensional tube which transitions from M_1^u to M_1^s which goes to S_R^2 . This implies P_0 returns to S_R^2 at a later time. Now, if M_1^u intersects M_1^s transversally, then these manifolds intersect in a complex manner, where the image of M_1^u on two-dimensional sections, $S_{\theta_i^s}$, are not circles, but parts of circles after several cycles of P_0 about P_1 . However, the separatrix property is still preserved, and P_0 still returns to S_R^2 [21].

Let's assume it returns to S_R^2 after a time T , ($t_2 = t_1 + T$). P_0 is a transit orbit and must pass through N_2 for $t > t_2$ into H_2 through the interior region bounded by M_2^u , where it is again weakly captured by P_2 . This follows since when P_0 passes through N_2 into H_2 , within the interior region bounded by M_2^u , it will intersect $S_L^2 \subset N_2$ in H_2 . The estimate obtained in (27) is also obtained at S_L^2 . This implies P_0 is captured by P_2 at $S_L^2 \subset N_2$ at a time $t_2 + \delta$, $\delta > 0$. Under the previous assumptions on capture points in theorem A, P_0 is weakly captured and weakly escapes P_2 .

The motion of P_0 as it leaves weak capture near P_2 , passing into the H_1 region and moving back to the H_2 to weak capture is illustrated in figure 6.

It is noted that there exists a time $\tilde{t}_3 < t_2$ where $E_2 > 0$, which follows from the proof of proposition 3.1. Thus, P_0 is weakly captured in backwards time at $t = t_2 + \delta$.

A similar argument holds for $C \lesssim C_1$. Within H_2 there are openings at N_1 to the left of P_2 and N_2 to the right. P_0 can now move into H_3 through N_1 , in addition to moving into H_1 through N_2 , from weak capture points on $W_k^u \cap \mathcal{L}$ in H_2 after j cycles. If P_0 moves into H_1 , it does so from the region bounded by $M_1^u(\gamma_2)$ and the same argument follows from the case $C \lesssim C_2$.

If P_0 moves about P_1 in H_3 , it moves in a bounded region \mathfrak{M}_3 . This region is bounded by $S_L^2 = \partial N_1$ in H_3 , a McGehee torus T_M about P_1 in H_3 and the boundary of H_3 . P_0 moves inside the region enclosed by $M_3^u(\gamma_1)$ and

⁶ T_M exists due to the fact that KAM tori on $\{J = C\}$ cannot exist too close to P_2 .

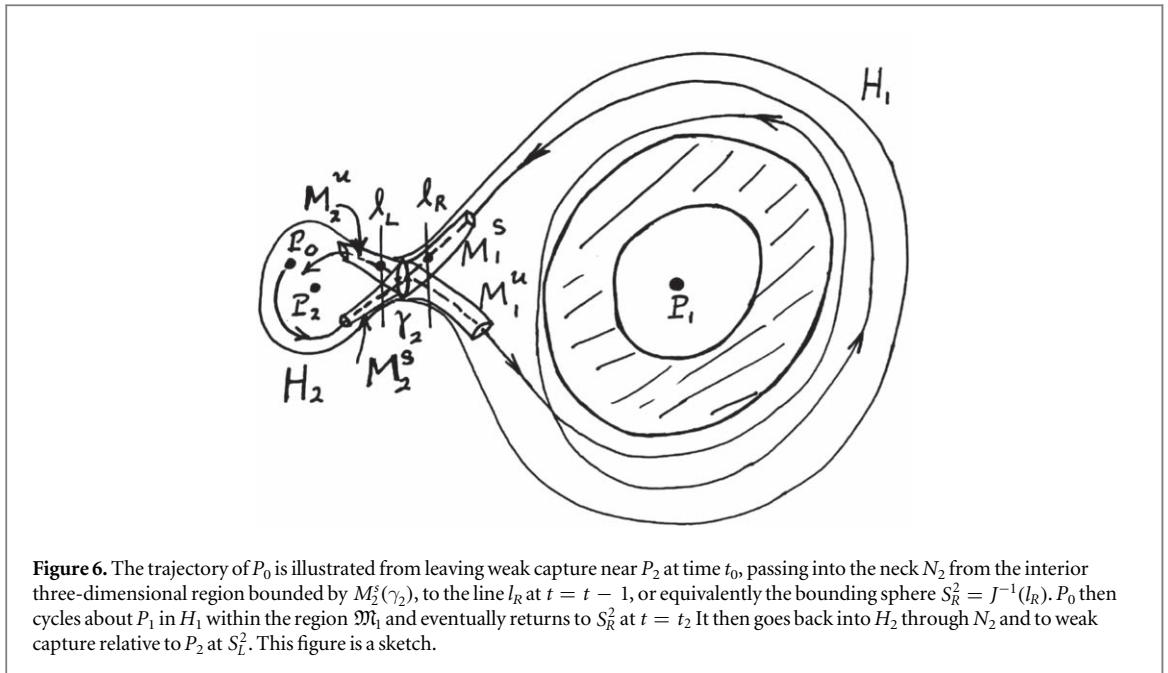


Figure 6. The trajectory of P_0 is illustrated from leaving weak capture near P_2 at time t_0 , passing into the neck N_2 from the interior three-dimensional region bounded by $M_2^s(\gamma_2)$, to the line l_R at $t = t - 1$, or equivalently the bounding sphere $S_R^2 = J^{-1}(l_R)$. P_0 then cycles about P_1 in H_1 within the region \mathfrak{M}_1 and eventually returns to S_R^2 at $t = t_2$. It then goes back into H_2 through N_2 and to weak capture relative to P_2 at S_L^2 . This figure is a sketch.

stays within it as this manifold either transitions into $M_3^s(\gamma_1)$ as a homoclinic tube or if the manifolds have transverse intersection. The separatrix property is satisfied, and P_0 will cycle about P_1 in H_3 j times until transits into H_2 and intersects $S_R^2 = \partial N_1$ in H_2 , where (27) is satisfied which implies P_0 is captured by P_2 at a time $t_2 + \delta$. Under the assumptions of theorem A, P_0 is weakly captured at P_2 .

It is noted P_0 is weakly captured in backwards time, since there is a time $t_3 < t_2$ where $E_2 > 0$, when P_0 was moving in H_3 , using the same argument as in the proof of proposition 3.1.

The final part of the proof of proposition 3.4 is to prove that P_0 moves in resonance orbits about P_1 .

We consider $C \lesssim C_2$, where P_0 is moving in H_1 . P_0 is on an approximate resonance orbit in H_1 about P_1 for $t_1 \leq t \leq T$. This is proven as follows: P_0 moves in \mathfrak{M}_1 . The orbit for P_0 will not deviate too much for μ sufficiently small, by the amount $\mathcal{O}(\mu^{1/3})$ [18]. It is an approximate elliptic Keplerian orbit about P_1 , since its energy $E_1 < 0$ (proven in the following text, see proposition A). It has a uniform approximate Keplerian period, T_1 , for μ sufficiently small, with approximate frequency $\omega_1 = T_1^{-1}$. Once P_0 moves away from S_R^2 for $t > t_1$, and returns to S_R^2 for $t = t_2 = T + t_1$. When P_0 returns to S_R^2 , it returns to near P_2 to approximately the distance $\mathcal{O}((\mu/3)^{2/3})$, as follows from the proof of proposition 3.3.

Since P_0 returns to S_R^2 , near to P_2 , T must approximately be an integer multiple, n , of the period, T_2 , of P_2 about P_1 . That is, $T \approx nT_2$. Also, since P_0 returns to near where it started, $T \approx mT_1$. Thus, $mT_1 \approx nT_2$. Equivalently, $n\omega_1 \approx m\omega$. Thus, P_0 moves in an approximate $n:m$ resonance with P_2 . It is noted that the approximate elliptic orbits of P_0 have an apoapsis distance from P_1 that is approximately the distance of S_R^2 to P_1 .

This can also be visualized in inertial coordinates, (Y_1, Y_2) centered at P_1 . When P_0 has started its motion on a near ellipse, for $t > t_1$, it has just left weak capture from near P_2 at the location, Y^* . P_0 then cycles about P_1 and keeps returning to near Y^* each approximate period T_1 . When it arrives near Y^* , P_2 needs to be nearby as when P_0 started its motion. Otherwise, P_0 won't become weakly captured by P_2 and leave the ellipse to move to the H_2 to weak capture by P_2 . In that case it will continue cycling about P_1 . If it does return to near Y^* and P_2 has also returned near to where it started also near Y^* , then this means P_2 has gone around P_1 approximately n times and P_0 has gone around P_1 approximately m times.

In the case where P_0 moves in the H_3 region after leaving S_L^2 for $t > t_1$, one also obtains a resonance orbit by an analogous argument. In this case, P_0 has a periapsis near $S_L^2 = \partial N_1$ with respect to P_1 , where $S_L^2 = \partial N_1$ is near P_2 at a distance of approximately, $\mathcal{O}((\mu/3)^{1/3})$. These resonance orbits in H_3 are much larger than the resonance orbits in H_1 since they move about both P_1, P_2 .

Proposition A. $E_1 < 0$ when P_0 moves in H_1 about P_1 in a resonance orbit.

Proof of proposition A. When P_0 moves for $t > t_1$ it moves in an approximate two-body manner for finite time spans, where the osculating eccentricity e_1 and semi-major axis a_1 vary only for a small amount amount by $\mathcal{O}(\mu^{1/3})$ since P_0 moves within \mathfrak{M}_1 . The energy E_1 is estimated (in an inertial frame). Since at $t = t_1$, $V_1(t_1) \approx 1 - |z(t_1)|$. We can estimate $|z(t_1)|$ as roughly the distance of L_2 to P_2 . This implies,

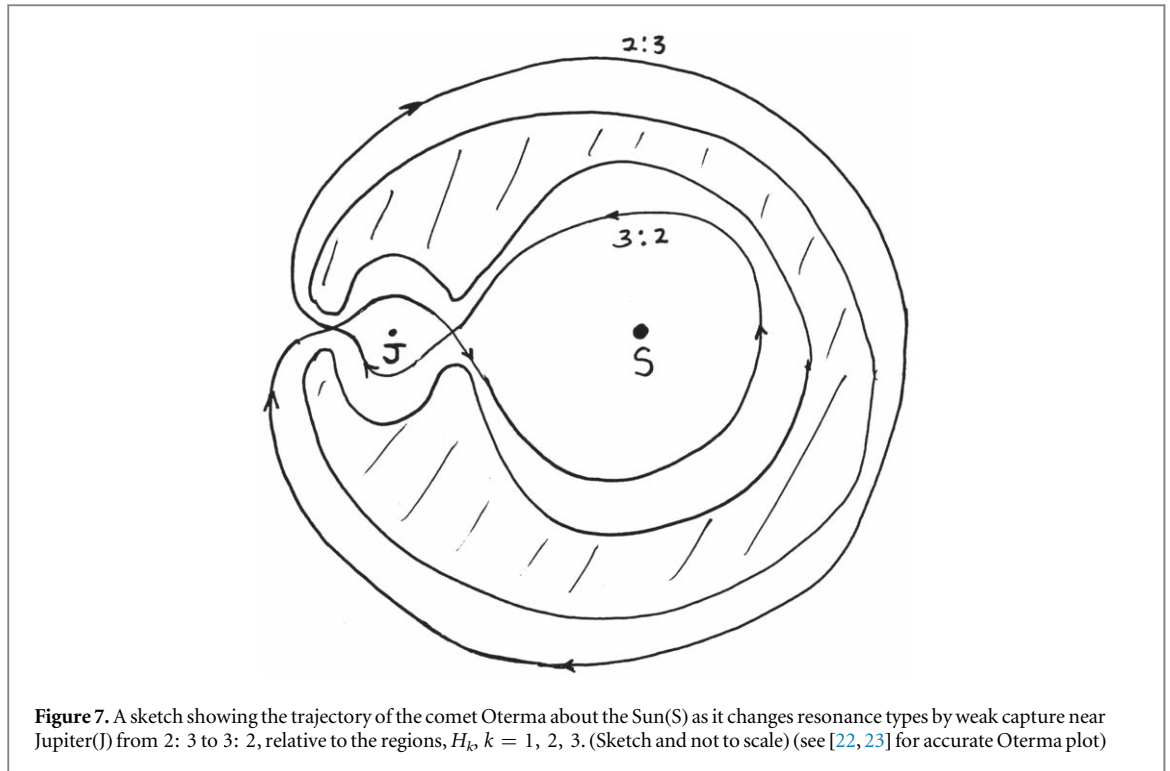


Figure 7. A sketch showing the trajectory of the comet Oterma about the Sun(S) as it changes resonance types by weak capture near Jupiter(J) from 2: 3 to 3: 2, relative to the regions, H_i , $k = 1, 2, 3$. (Sketch and not to scale) (see [22, 23] for accurate Oterma plot)

$|z(t_1)| \approx \alpha^{1/3} + \mathcal{O}(\alpha^{2/3})$, $\alpha = \mu/3$, and $r_1 \approx 1 - \alpha^{1/3} + \mathcal{O}(\alpha^{2/3})$. Thus,

$$E_1 \approx (1/2)(1 - \alpha^{1/3} + \mathcal{O}(\alpha^{2/3})^2 - (1 - \mu)(1 - \alpha^{1/3} + \mathcal{O}(\alpha^{2/3}))^{-1}. \tag{28}$$

Thus $E_1 \approx -(1/2) + \mathcal{O}(\alpha^{1/3})$. This implies that $E_1 < 0$ for μ sufficiently small. P_0 will then be moving on an approximate ellipse about P_1 of an eccentricity, $e_1 < 1$. The apoapsis of this ellipse will approximately be $r_a \approx r_1(t_1) \approx 1 - (\mu/3)^{1/3}$. The semi-major axis of the ellipse at $t = t_1$ is approximately, $a_1 \approx -(1 - \mu)/(2E_1) \approx (1 - \mu) + \mathcal{O}((\mu/3)^{1/3})$. $e_1 \approx 1 - (r_a/a_1) < 1$.

When P_0 moves in resonance orbits in H_3 for $C \lesssim C_1$, similar estimates are made where $E_1 < 0$.

End of proof of proposition A.

The resonance orbits of P_0 about P_1 move in an approximate two-body fashion where the perturbation due to P_2 is negligible for finite time spans. Thus, $\omega_1(t) \approx (m/n)\omega$ until it enters either neck to move to weak capture near P_2 .

We assume $C \lesssim C_2$ and examine what happens to the motion of P_0 near Y^* when in $n: m$ resonance with P_2 . P_0 is at a minimal distance to P_2 when near Y^* . In the rotating system, it is near S_R^2 , and lies in the three-dimensional region contained within M_1^s , since it has been moving about P_1 within this region by the separatrix property. At this minimal distance, M_1^s is close enough to γ_2 so that it can connect with it, and P_0 can move as a transit orbit and move through N_2 and exit into H_1 through the three-dimensional interior region bounded by M_1^u . It is then captured by P_2 , with $E_2 \lesssim 0$ at S_L^2 . An analogous argument holds when $C \lesssim C_1$.

Assuming the generic assumptions are satisfied for theorem A, P_0 will weakly escape P_2 and again move into H_1 , or H_3 , obtaining resonance orbits, satisfying, $\omega_1 \approx (m'/n')\omega$, for integers $n' \geq 1$, $m' \geq 1$. The set of all such resonance orbits forms the family \mathfrak{F} . This concludes the proof of theorem A.

An example of the geometry of resonance transitions for an observed comet, Oterma, from a 2: 3 to a 3: 2, in 1936, and then back from a 3: 2 to a 2: 3, in 1962, ([22, 23]) is illustrated in figure 7. (See section 3.1 at the end of this section.)

It is noted that the estimates of E_1 , E_2 in the proof of theorem 2 while P_0 moves in H_i , $i = 1, 2, 3$, are observed in the motions of the resonating comets studied in [22]. It can be seen in [22] that when the comet Gehrels 3 was weakly captured by Jupiter(P_2) from a 2:3 resonance orbit into an approximate 3:2 resonance orbit, $E_2 \lesssim 0$. Also, when the comet moved about the Sun(P_1) in an approximate 2:3 resonance orbit, $E_2 > 0$ and $E_1 < 0$.

For each resonance orbit obtained from the choice of the weak capture initial condition, (6) is satisfied, proving lemma A.

3.1. Examples of resonance orbits in \mathfrak{F} and \mathfrak{U} .

Result A describes a dynamical mechanism of resonance orbits about P_1 . The resonance motion described in this paper is observed both in nature and numerically.

It was originally inspired by the fact that comets are observed to perform it. More exactly, there exists a special set of comets that move about the Sun that transition between approximate resonance orbits about the Sun due to weak capture at Jupiter. This is studied in [22–24]. Several comets are described in [22, 24], that perform this motion. For example, the comet *Oterma* transitions between a 3:2-resonance with respect to the Sun, where $\omega_1 = (2/3)\omega$, ω is the frequency of Jupiter, to a 2:3-resonance. When passing between these resonances, the comet, P_0 , is weakly captured by Jupiter. There are many others, listed in [22] (table 1), and in [24]. These comets include Helin-Roman-Crockett (3: 2 \rightarrow 3: 2), Harrington-Abell (5: 3 \rightarrow 8: 5). It is important to note that the modeling used to describe the resonance orbits of these comets is not exactly the model used in this paper. It models the true orbit of Jupiter about the Sun using the planetary ephemeris and the observed orbits of the comets for initial conditions which are not exactly planar. This model is very close to the planar restricted three-body problem. The definition of approximate resonance orbits in this paper for the restricted three-body problem is well suited to the resonances comets perform.

The existence of orbits performing resonance transitions as in \mathfrak{F} can also be found in the planar circular restricted three-body problem used in this paper. A special case where the resonance orbit precisely returns to its initial condition after performing a transition was shown to exist in [25]. This yields an exact periodic orbit that repeats the same transition over and over. Other simulations of approximate resonance orbits as in \mathfrak{F} for the planar circular restricted three-body problem and models very close to that model are done in [26, 27].

An interesting example of orbits that occur in nature can be obtained for \mathfrak{U} given in Result C. These are the subset of resonance transition orbits that have frequencies, $\omega_1(m/n) \approx (m/n)\omega$, $m = 8$, $n = \tilde{n}^3$, $\tilde{n} = 1, 2, \dots$. That is, the orbits have \tilde{n}^3 : 8 resonances. A special case of these resonances is an 8: 8 resonance for $\tilde{n} = 2$. On the other hand, a 1: 1 resonance orbit is a special case of an 8: 8 resonance orbit. An example of this is for the Trojan asteroids, where P_1 is the Sun, P_2 is Jupiter, and P_0 is a Trojan asteroid. Many other examples can be found by asteroids located near the equilateral Lagrange points with respect to a body P_2 , orbiting P_1 .

4. Modeling resonance motions with the modified Schrödinger equation

In this section some of the results are expanded upon in section 2.

The family \mathfrak{F} of resonance periodic orbits, $\Phi_{m/n}$, are modeled in the plane by the restricted three-body problem. The planar modeling is justified in section 3. To try and model \mathfrak{F} with quantum mechanical ideas, we therefore use planar modeling. Thus, we consider the planar, time independent, modified Schrödinger equation given in the Introduction by (1), obtained from the classical Schrödinger equation, (?), by replacing \hbar by σ , and the potential is given by the three-body potential \bar{V} derived from the planar restricted three-body problem. This partial differential equation is time independent.

The motivation of replacing \hbar by σ is given by analogy A in section 2, where σ given by (11). The potential \bar{V} is given by (15), obtained from $\hat{V} = V_1 + V_2$. It is recalled that V_1 is the potential due to P_1 and V_2 is the potential due to P_2 , in an inertial P_1 -centered coordinate system, (Y_1, Y_2) . It is also recalled that P_2 moves about P_1 on the circular orbit, $\gamma(t)$, $m_0 \gtrsim 0$, and as described in section 2 for Results A, it is necessary that m_0, m_2 are sufficiently small for the approximations in assumptions 1.

As described in section 2 the modified Schrödinger equation is given by (16), where \bar{V} is the average of \hat{V} , obtained by averaging V_2 over a cycle of P_2 about P_1 on γ , given by (14). For reference, we recall (16),

$$-\frac{\sigma^2}{2\nu}\nabla^2\Psi + \bar{V}\Psi = E\Psi, \quad (29)$$

In the macroscopic scale for the masses, and relative distances, two dimensions is required, where, in the inertial P_1 -centered coordinates, (Y_1, Y_2) $\nabla^2 \equiv \frac{\partial^2}{\partial Y_1^2} + \frac{\partial^2}{\partial Y_2^2}$. When solving (29), the three-dimensional problem is solved for generality. The three-dimensional problem is discussed when considering the quantum scale.

It is noted that the units of σ are $m^2\text{kg}s^{-4/3}$. This needs to match the units of \hbar which are $m^2\text{kg}s^{-1}$. ($\hbar = 6.626\ 07 \times 10^{-34}m^2\text{kg}s^{-1}$) Thus, we need to multiply σ by $\rho = 1s^{1/3}$, $\sigma^* = \rho\sigma$. σ^* has the same units as \hbar . Keeping the same notation, $\sigma^* \equiv \sigma$. At the end of this section it is seen that when the masses approach the quantum scale, σ also gets small, and m_0, m_1 can be adjusted so that $\sigma = \hbar$.

We recall (15), $\bar{V} = V_1 + \bar{V}_2$, where $V_1 = -Gm_0m_1/r$, $r = |Y|$ and \bar{V}_2 is the time average of $V_2 = -Gm_0m_2/r_2$, $r_2 = |Y - \gamma(t)|$. It is shown in this section, \bar{V}_2 is given by (48) which has a form similar to V_1 . This enables solving (16).

The solution to (29) is done in two steps. In the first step, we solve (29) in the absence of gravitational perturbations due to P_2 for $m_2 = 0$, where $\bar{V}_2 = 0$. Thus, in this case $\bar{V} = V_1$. It is then solved for $m_2 > 0$ where

\bar{V}_2 is non-zero. (Since the form of \bar{V}_2 is shown to have a form analogous to V_1 , we can modify the solution obtained for V_1 for the addition of \bar{V}_2 .)

We explicitly solve (29), with $m_2 = 0$, by separation of variables. This is for the two-body motion of P_0 about P_1 . It is first solved for three-dimensions, then restricted to the planar case studied in this paper for the macroscopic scale. The three-dimensional solution is referred to when discussing solutions in the quantum scale. (29) is transformed to spherical coordinates, r, ϕ, θ . It is assumed the solution is of the form,

$$\Psi = R(r) Y(\phi, \theta). \tag{30}$$

$r \geq 0$, and ϕ is the angle relative to the Y_1 -axis, $0 \leq \phi \leq 2\pi$. θ is the angle relative to the Y_3 -axis, $0 \leq \theta \leq \pi$. $|\Psi|^2$ is the probability of finding P_0 at distance r from P_1 .

The solution of (29) for $\bar{V}_2 = 0$ follows the method described in [28] for the case of an electron in the Hydrogen atom moving about the nucleus. This is a standard approach used in solving the classical Schrödinger equation in quantum mechanics found in many references. There are some minor modifications. The Coulomb potential is used in [28] for V_1 and here we are using the gravitational potential between two particles P_0, P_1 ; however, they are of the same form, both proportional to r^{-1} , $r^2 = Y_1^2 + Y_2^2 + Y_3^2$. Instead of the proportionality term of Gm_0m_1 , the Coulomb potential has the term, $Ze^2q_1/(4\pi\epsilon_0)$, where Z is the atomic number, $Z = 1$ for Hydrogen, e is the charge of the electron and the charge of the nucleus, P_0 and an atomic nucleus, P_1 , ϵ_0 is the permittivity of vacuum, \hbar is replaced by σ . The reduced mass $\nu = m_0m_1/(m_0 + m_1)$ is defined for either the gravitational or Coulomb modeling. When referring to [28], one replaces $e^2/(4\pi\epsilon_0)$ by Gm_0m_1 .

When solving (29) by separation of variables, (30) is substituted into (29), obtaining differential equations for $R(r)$ and $Y(\phi, \theta)$,

$$\frac{d^2R}{dr^2} + 2r^{-1}\frac{dR}{dr} + [2\nu\sigma^{-2}(E + Gm_0m_1r^{-1}) - \alpha r^{-2}]R = 0, \tag{31}$$

$$(\sin \theta)^{-1} \frac{\partial}{\partial \theta} \left(\sin \theta \frac{\partial Y}{\partial \theta} \right) + (\sin \theta)^{-2} \frac{\partial^2 Y}{\partial \phi^2} + \alpha Y = 0. \tag{32}$$

α is a separation constant.

(32) is solved first, yielding spherical harmonics. Using separation of variables, solutions are obtained in the form, $Y(\phi, \theta) = \Phi(\phi)\Theta(\theta)$. This gives the differential equations,

$$\Theta^{-1} \sin \theta \frac{d}{d\theta} \left(\sin \theta \frac{d\Theta}{d\theta} \right) + \alpha \sin^2 \theta - \beta = 0, \tag{33}$$

$$\frac{d^2\Phi}{d\phi^2} + \beta\Phi = 0, \tag{34}$$

where β is a separation constant [28].

(34) gives the solution,

$$\Phi(\phi) \equiv \Phi_{m_l}(\phi) = (1/2\pi)^{1/2} e^{im_l\phi}, \tag{35}$$

$\beta = m_l^2$, $m_l = 0, \pm 1, \pm 2, \dots, i^2 = -1$. $\Phi(\phi)$ varies in the Y_1, Y_2 -plane.

The solution of (33) follows by setting $x = \cos \theta$, $G(x) \equiv \Theta(\cos x)$ transforming (33) into an associated Legendre type differential equation,

$$(1 - x^2) \frac{d^2G}{dx^2} - 2x \frac{dG}{dx} + (\alpha - m^2(1 - x^2)^{-1})G = 0, \tag{36}$$

$\alpha = l(l + 1)$, $l = |m_l|, |m_l| + 1, |m_l| + 2, \dots$ [28]. l varies between $\pm|m_l|$. The solutions of (36) are given by associated Legendre polynomials $P_{l,|m_l|}(x)$. (see [29] for tables of these polynomials) The solutions of (33) are given by ([28], page 527),

$$\Theta_{l,m_l}(\theta) = \left[\left(\frac{2l + 1}{2} \right) \frac{1 - |m_l|!}{1 + |m_l|!} \right]^{1/2} P_{l,|m_l|}(\cos \theta). \tag{37}$$

It is remarked that in the two-dimensional problem, with coordinates (Y_1, Y_2) , $\theta = \pi/2$. In this case, there is no variation with respect to θ and Θ is only defined at $\theta = \pi/2$.

The solution $Y(\phi, \theta)$ is given by the spherical harmonics $Y_{l,m_l} = \Phi_{m_l}(\phi)\Theta_{l,m_l}(\theta)$. To solve (31), set $u = Rr$. (31) becomes,

$$\frac{d^2u}{dr^2} + (\tilde{a}r^{-1} - br^{-2})u = \lambda^2u, \tag{38}$$

where $\lambda^2 = 2\nu|E|\sigma^{-2}$, $\tilde{a} = 2\nu\sigma^{-2}Gm_0m_1$, $b = l(l + 1)$. It is verified that solving this differential equation yields the solution of (31),

$$R \equiv R_{\tilde{n},l}(r) = - \left[\frac{2 \left((\tilde{n} - l - 1)! \right)}{\tilde{n} \left(2\tilde{n}[(\tilde{n} + l)!]^3 \right)} \right] \rho^l L_{\tilde{n}+l}^{l+1}(\rho) e^{-\rho/2}, \tag{39}$$

where, $\tilde{n} = 1, 2, \dots, l = 1, \dots, \tilde{n} - 1, \rho = (2/(\tilde{n}a))r, a = (\nu Gm_0 m_1)^{-1} \sigma^2$, and L_j^l are the associated Laguerre polynomials ([28], page 8, table 3.2), and

$$E \equiv \hat{E}_{\tilde{n}} = - \frac{2\nu\pi^2 (Gm_0 m_1)^2}{\sigma^2 \tilde{n}^2}. \tag{40}$$

E can be written as,

$$\hat{E}_{\tilde{n}} = - \frac{4\sigma}{\tilde{n}^2}. \tag{41}$$

This follows by the identity,

$$2\nu\pi^2 \tilde{\rho}^2 \sigma^{-3} = 4, \tag{42}$$

where $\tilde{\rho} = Gm_0 m_1$.

The solution for E yields quantized values of the energy, which quantizes the gravitational field between P_0, P_1 .

The general solution to (29) is given by multiplying (39) with Y_{l,m_l} ,

$$\Psi(r, \phi, \theta) \equiv \Psi_{\tilde{n},m_l,l} = R_{\tilde{n},l}(r) \Phi_{m_l}(\phi) \Theta_{l,m_l}(\theta). \tag{43}$$

\tilde{n}, l, m_l are the quantum numbers associated with Ψ . \tilde{n} is called the principle quantum number and is independent of l, m_l . It specifies the energy value and limits the value of l . The quantum numbers l, m_l occur by consideration of the spherical harmonics.

We compute the probability distribution function, F , of locating P_0 relative to P_0 at a given point (r, ϕ, θ) . Since we are currently considering the masses and the relative distances to be macroscopic, this probability is used to measure the location of a macroscopic particle, and not as a wave as is done in the quantum scale, that is considered later in this section. By definition, $F(r, \phi, \theta) = |\Psi_{\tilde{n},m_l,l}(r, \phi, \theta)|^2$, depending on the quantum numbers.

It is more convenient to compute the probability at a given radial distance r , independent of ϕ, θ . It is labeled $P(r)$.

It is verified that $P(r) = R^2 r^2$. This is valid in the two-dimensional case as well for (Y_1, Y_2) .

As an example, calculate $P(r)$ at the lowest energy value corresponding to $\tilde{n} = 1, l = 0$.

$$P(r) = 4a^{-3} r^2 e^{-2r/a}. \tag{44}$$

(see [28], table 3.2, where a is given in the Hydrogen atom case). It is verified that $P(r)$ has a maximum at $r = a$, with $P(0) = 0$ and where $P(r) \rightarrow 0$ as $r \rightarrow \infty$. It yields a curve $\{(r, P(r)) | r \in [0, \infty]\}$ analogous to the Hydrogen atom case (see [28], figure 3.20). The numerical values of $P(r)$ will differ from the Hydrogen atom case, since in the gravitational case $a = (\nu Gm_0 m_1)^{-1} \sigma^2$.

The maximum of the distribution function at $r = a$ says that P_0 , as a macroscopic body, has the highest probability of being located at this distance. In the case of the Hydrogen atom, where P_0 has wave-particle duality, this distance corresponds to the Bohr radius, which is the most probable location to find an electron in general, referred to as the 1s-orbital (s denotes $l = 0$).

In the same way, $P(r)$ can be computed for $\tilde{n} = 1, 2, \dots, l = 0, 1, 2, \dots, \tilde{n} - 1$, which determines most probable radial locations for P_0 to be located.

If one considers computing $F(r, \phi, \theta) = |\Psi_{\tilde{n},m_l,l}(r, \phi, \theta)|^2$ over \tilde{n}, l, m_l , where $-|m_l| \leq l \leq |m_l|$, then one obtains precise regions about P_1 where P_0 is most probable to be located. These are well known in the case of the Hydrogen atom [28]. It is remarkable these are observed to occur. In the gravitational case considered in this paper, the regions will have a similar geometry, but with different scaling.

The solution of (29) has been obtained in three dimensions for $m_2 = 0$. We solve this for $m_2 > 0, m_2 \ll m_1$, and then reduce to the planar case in order to compare to the planar restricted three-body problem in the macroscopic scale.

When the gravitational perturbation due to P_2 is included, the previous results are obtained with a small perturbation. It is also seen that the frequencies $\omega_1(\tilde{n})$ correspond to the subset, \mathfrak{A} , of the resonant family \mathfrak{F} .

Three-body potential

The previous analysis can be done for a more general three-body potential by taking into account the gravitational perturbation due to P_2 . We do this by using an averaged potential, \bar{V}_2 , obtained from the potential V_2 , due to the gravitational interaction of P_0, P_2 . This yields the three-body potential, $\bar{V} = V_1 + \bar{V}_2$ that approximates $\hat{V} = V_1 + V_2$. This is done as follows,

We do this analysis in three-dimensional inertial coordinates, $Y = (Y_1, Y_2, Y_3)$, centered at P_1 , P_2 moves about P_1 on a circular orbit of radius β , and angular frequency ω , in the (Y_1, Y_2) -plane, $\gamma(t) = \beta(\cos \omega t, \sin \omega t, 0)$, β is a constant. The potential for P_0 due to the perturbation of P_2 is given by

$$\hat{V} = V_1 + V_2 = -\frac{Gm_0m_1}{r} - \frac{Gm_0m_2}{r_2}, \quad (45)$$

where $r = |Y|$, $r_2 = |Y - \gamma(t)|$. We can write r_2 as

$$r_2 = \sqrt{r^2 + \beta^2 - 2\beta(Y_1 \cos \omega t + Y_2 \sin \omega t)},$$

We consider V_2 and take the average of it over one cycle of P_2 , where $t \in [0, 2\pi/\omega]$,

$$\bar{V}_2 = -\frac{Gm_0m_2\omega}{2\pi} \int_0^{\frac{2\pi}{\omega}} \frac{dt}{\sqrt{r^2 + \beta^2 - 2\beta(Y_1 \cos \omega t + Y_2 \sin \omega t)}}. \quad (46)$$

This averaged potential term is an approximation to V_2 , representing the average value of V_2 felt by P_0 at a point (Y_1, Y_2, Y_3) over the circular orbit of P_2 about P_1 in the (Y_1, Y_2) -plane. It is advantageous to use since it eliminates the time dependence in V_2 , and as we'll show, can be written so that it approximately takes the form of V_1 . This implies we can solve (29) as before, with minor modifications. Approximating V_2 in this way yields \bar{V}_2 .

Expressing Y_1, Y_2 in polar coordinates, $Y_1 = r \cos \theta$, $Y_2 = r \sin \theta$, and making a change of the independent variable, $t, \phi = \omega t$, we obtain

$$\bar{V}_2 = -\frac{Gm_0m_2}{2\pi} \int_0^{2\pi} \frac{d\phi}{\sqrt{r^2 + \beta^2 - 2\beta r \cos(\phi - \theta)}}. \quad (47)$$

\bar{V}_2 is simplified by considering three cases, $r < \beta$, and $r > \beta$, $r = \beta$, and expanding \bar{V}_2 as a binomial series. We prove,

Summary A. The general three-body potential $\hat{V} = V_1 + V_2$, (12), for P_0 can be approximated by replacing V_2 , due to the perturbation of P_2 , with the averaged potential \bar{V}_2 , (47). \bar{V}_2 can be written as,

$$\bar{V}_2 = \begin{cases} -Gm_0m_2r^{-1} + \mathcal{O}(m_0m_2), & r > \beta \\ -Gm_0m_2\beta^{-1} + \mathcal{O}(m_0m_2), & r < \beta \\ -Gm_0m_2\frac{1}{\sqrt{2}}r^{-1} + \mathcal{O}(m_0m_2), & r = \beta. \end{cases} \quad (48)$$

The quantized energy, $\hat{E}_{\tilde{n}}$, for the approximated three-body potential $\bar{V} = V_1 + \bar{V}_2$ is given by,

$$\hat{E}_{\tilde{n}} = \begin{cases} -4\sigma\tilde{n}^{-2}(1 + \mu + \mu^2) + \mathcal{O}(m_0m_2), & r > \beta \\ -4\sigma\tilde{n}^{-2} - Gm_0m_2\beta^{-1} + \mathcal{O}(m_0m_2), & r < \beta \\ -4\sigma\tilde{n}^{-2}(1 + \frac{1}{\sqrt{2}}\mu + \frac{1}{2}\mu^2) + \mathcal{O}(m_0m_2), & r = \beta \end{cases} \quad (49)$$

which reduces to (41) for $m_2 = 0$, and where $\mu = m_2/m_1$.

From the form of σ , (49) implies,

$$\hat{E}_{\tilde{n}} = -4\sigma\tilde{n}^{-2} + \mathcal{O}(m_0m_2). \quad (50)$$

Similarly,

Summary B.

$$R_{\tilde{n},l}(r) = -\left[\frac{2}{\tilde{n}} \left(\frac{(\tilde{n} - l - 1)!}{2\tilde{n}[(\tilde{n} + l)!]^3} \right) \right] \rho^l L_{\tilde{n}+l}^{l+1}(\rho) e^{-\rho/2} + \mathcal{O}(m_0m_2), \quad (51)$$

for $r \geq \beta$, $r < \beta$. The probability distribution function is generalized to,

$$P(r) = R^2(r)r^2 + \mathcal{O}(m_0m_2). \quad (52)$$

When adding the gravitational perturbation due to P_2 represented by \bar{V}_2 , one obtains smooth dependence on this term in all the calculations. This proves summary B.

Equivalence of solutions of the modified Schrödinger equation with the family \mathfrak{F} of the three-body problem

The two-dimensional case is now considered to compare the solutions of the modified Schrödinger equation, (29), to the family of solutions \mathfrak{F} of the planar restricted three-body problem.

We set $Y_3 = 0, \theta = \pi/2$. The quantized energy $\hat{E}_{\tilde{n}}$, (41), for (29) of the two-body motion of P_0 about P_1 , with $m_2 = 0$, is not defined in the same way as the two-body Kepler energy \tilde{E}_1 , (10). $\hat{E}_{\tilde{n}}$ is computed from the modified Schrödinger equation and \tilde{E}_1 is computed for the Kepler problem for general elliptic motion of P_0 about P_1 . These are different expressions. However, they both represent the energy of P_0 for the two-body gravitational potential. Also, $\hat{E}_{\tilde{n}}$ is quantized and \tilde{E}_1 is not quantized.

A key observation of this paper is that when one solves for the Kepler frequency ω_1 in (10) as a function of \tilde{E}_1 and substitutes $\hat{E}_{\tilde{n}}$ in place of \tilde{E}_1 , a simple equation is obtained for ω_1 ,

$$\omega_1|_{\tilde{E}_1=\hat{E}_{\tilde{n}}} \equiv \omega_1(\tilde{n}) = 8\tilde{n}^{-3}. \tag{53}$$

It is remarked that this equation is also valid in three-dimensions since (10) is also valid for the three-dimensional Kepler two-body problem.

This follows by noting that (10) implies,

$$\omega_1 = [-\sigma^{-1}\tilde{E}_1]^{3/2}. \tag{54}$$

This yields (53)

Inclusion of gravitational perturbation of P_2 ($m_2 > 0$), implies more generally,

$$\omega_1|_{\tilde{E}_1=\hat{E}_{\tilde{n}}} \equiv \omega_1(\tilde{n}) = 8\tilde{n}^{-3} + \mathcal{O}(m_0m_2). \tag{55}$$

(53) does not depend on the masses or any other physical parameter. This says substituting the quantized energy from the modified Schrödinger equation, with $m_2 = 0$, into the Kepler energy for the frequency, yields a frequency of motion for P_0 moving about P_1 in elliptical orbits that is same for all masses only depending on the wave number \tilde{n} . This discretizes the Kepler frequencies.

The discretization of the Kepler frequencies restricts the elliptical two-body motion of P_0 . This result becomes relevant in the three-body problem for \mathfrak{F} when the gravitational perturbation P_2 is included since it selects a the set of resonance orbits, $\mathfrak{U} \subset \mathfrak{F}$ (see result C, section 2).

We prove result C from section 2, which we state as $\omega_1(\tilde{n})$, given by (55), which are the frequencies in the restricted three-body problem corresponding to the modified Schrödinger equation energies, form a subset $\mathfrak{U} \subset \mathfrak{F}$ of resonance orbits where $m = 8, n = \tilde{n}$.

Proof of result C. This is proven by first noting that the circular restricted three-body problem can rescaled so that $m_1 = 1 - \mu, m_2 = \mu, G = 1, \beta = 1$ where $\mu = m_2/(m_1 + m_2)$ [8]. This scaling does not reduce the generality of the mass values nor β . This scaling implies $\omega = 1$. Thus, (6) becomes,

$$\omega_1(m/n) = (m/n) + \mathcal{O}(\delta). \tag{56}$$

A key observation is that this scaling does not effect the leading term $8/\tilde{n}^3$ of $\omega_1(\tilde{n})$ given by (55). Thus, after the scaling, subtracting (55) from (56) yields,

$$\omega_1(m/n) - \omega_1(\tilde{n}) = \frac{m}{n} - \frac{8}{\tilde{n}^3} + \mathcal{O}(m_0m_2). \tag{57}$$

Thus, taking $m = 8, n = \tilde{n}^3$ and assuming m_2 is sufficiently small, implies,

$$\omega_1(m/n) \approx \omega_1(\tilde{n}), \tag{58}$$

This condition is preserved by rescaling to general m_1, m_2, β , yielding $\omega_1(m/n) \approx (8/\tilde{n}^3)\omega$ for \mathfrak{U} .

From the macro to quantum scale

When m_0, m_2, m_3 are in the macroscopic scale then as described in section 2, in results B and C, the family $\mathfrak{U} \subset \mathfrak{F}$ of near resonance orbits can be described by the solution (17) of (29).

For the masses in the quantum scale, the family \mathfrak{U} are no longer valid. Ψ given by (17) is still valid but now as pure wave solutions. This is summarized in result D, section 2. Thus, Ψ is defined for both macroscopic and quantum scales. In the macroscopic scale, Ψ is interpreted as a probability, whereas in the quantum scale, Ψ is a pure wave solution. The quantized energies $\hat{E}_{\tilde{n}}$ are still well defined. \mathcal{P} is still defined and yields the single domain \mathcal{D} , for $\tilde{n} = 1, 2, 3, \dots$ This is discussed in section 2.

This section is concluded with an analysis of σ , referred to in section 2.

Proposition 4.1 $\sigma = \hbar$ is satisfied for a one-dimensional algebraic curve (59) in (m_0, m_1) -space. This is proven by noting $\sigma = (1/2)(2\pi G)^{2/3}m_0m_1(m_0 + m_1)^{-1/3} < (1/2)(2\pi G)^{2/3}m_0m_1m_0^{-1/3}$. Hence, $\sigma < (1/2)(2\pi G)^{2/3}m_0^{2/3}m_1$. Thus, $\sigma \rightarrow 0$ as $m_0, m_1 \rightarrow 0$. This implies there exists values of m_0, m_1 such that $\sigma = \hbar$. This is equivalent to the equation,

$$m_0^3m_1^3 - \hbar a^{-3}(m_0 + m_1) = 0, \tag{59}$$

$a = (1/2)(2\pi G)^{2/3}$. (59) yields a one-dimensional algebraic curve, Γ , in the coordinates m_0, m_1 . This proves proposition 4.1.

The relevancy of possible wave motions for (m_0, m_1) not on Γ , with m_0, m_1, m_2 in the quantum scale, is not considered in this paper. This is discussed in section 2. Different models are also discussed in section 2.

Acknowledgments

I would like to acknowledge the support of Alexander von Humboldt Stiftung of the Federal Republic of Germany that made this research possible, and the support of the University of Augsburg for his visit from 2018–19. I would like to thank Urs Frauenfelder of the University of Augsburg for many interesting discussions. Research by E.B. was partially supported by NSF grant DMS-1814543. Special thanks to Marian Gidea of Yeshiva University for helpful discussions and figure 2. Also, thanks to David Spergel of Princeton University.

Appendix. Proof of summary A

Summary A is proven as follows: the integrand, I , of \bar{V}_2 is given by

$$I = \frac{1}{\sqrt{r^2 + \beta^2 - 2\beta r \cos(\phi - \theta)}} = \frac{1}{\sqrt{r^2 + \beta^2}} \frac{1}{\sqrt{1 - \frac{2\beta r}{r^2 + \beta^2} \cos(\phi - \theta)}}. \tag{60}$$

Case 1: $r > \beta$

This implies,

$$\frac{1}{\sqrt{r^2 + \beta^2}} = \frac{1}{r\sqrt{1 + \frac{\beta^2}{r^2}}} = \frac{1}{r}(1 + \mathcal{O}(x)), \tag{61}$$

where $x = \beta/r < 1$. This results from expanding the fraction containing the square root into a binomial series. Likewise, we can also expand the first term on the right in (60) in a binomial expansion since $|\cos(\phi - \theta)| \leq 1$ and

$$\frac{2\beta r}{r^2 + \beta^2} < 1, \tag{62}$$

yielding

$$\frac{1}{\sqrt{1 - \frac{2\beta r}{r^2 + \beta^2} \cos(\phi - \theta)}} = 1 + \mathcal{O}(y), \tag{63}$$

where

$$y = \frac{2\beta r}{r^2 + \beta^2} (\cos(\phi - \theta)), \tag{64}$$

$|y| < 1$. Thus, (60) becomes,

$$I = \frac{1}{r}(1 + \mathcal{O}(w)), \tag{65}$$

$|w| < 1, w = \max\{x, y\}$. Thus, in this case,

$$\bar{V}_2 = -\frac{Gm_0m_2}{r}(1 + \mathcal{O}(w)) = -\frac{Gm_0m_2}{r} + \mathcal{O}(m_0m_2). \tag{66}$$

This implies in the derivation of $\hat{E}_{\bar{n}}$, we proceed as before and replace the numerator Gm_0m_1 of V_1 in (31) with $Gm_0(m_1 + m_2)$ and adding $\mathcal{O}(m_0m_2)$ to this term. This yields,

$$\hat{E}_{\bar{n}} = -\frac{2\nu\pi^2(Gm_0(m_1 + m_2))^2}{\sigma^2\bar{n}^2} + \mathcal{O}(m_0m_2) \tag{67}$$

This can be written as,

$$\hat{E}_{\bar{n}} = -\frac{4\sigma}{\bar{n}^2}(1 + \mu + \mu^2) + \mathcal{O}(m_0m_2), \tag{68}$$

where $\mu = m_2/m_1$, and where we have used (42).

Case 2: $r < \beta$

This case is done in a similar way as in Case 1. Instead of factoring out r^{-1} from (61), we factor out β^{-1} , which yields,

$$\frac{1}{\sqrt{r^2 + \beta^2}} = \frac{1}{\beta\sqrt{1 + \frac{r^2}{\beta^2}}} = \frac{1}{\beta}(1 + \mathcal{O}(\tilde{x})), \tag{69}$$

where $\tilde{x} = r/\beta < 1$. Proceeding as in Case 1, we obtain,

$$I = \frac{1}{\beta}(1 + \mathcal{O}(\tilde{w})), \tag{70}$$

$|\tilde{w}| < 1$, $\tilde{w} = \max\{\tilde{x}, y\}$. This implies,

$$\tilde{V}_2 = -\frac{Gm_0m_2}{\beta}(1 + \mathcal{O}(\tilde{w})) = -\frac{Gm_0m_2}{\beta} + \mathcal{O}(m_0m_2). \tag{71}$$

Since β is a constant, then in the derivation of $\hat{E}_{\tilde{n}}$, we replace E with $E + (Gm_0m_2/\beta) + \mathcal{O}(m_0m_2)$ in (31) keeping V_1 as was used in the case of $m_2 = 0$ in (31). This yields,

$$\hat{E}_{\tilde{n}} = -\frac{2\nu\pi^2(Gm_0m_1)^2}{\sigma^2\tilde{n}^2} - \frac{Gm_0m_2}{\beta} + \mathcal{O}(m_0m_2) \tag{72}$$

This can be reduced to,

$$\hat{E}_{\tilde{n}} = -\frac{4\sigma}{\tilde{n}^2} - \frac{Gm_0m_2}{\beta} + \mathcal{O}(m_0m_2). \tag{73}$$

Case 3: $r = \beta$

In this final case,

$$\frac{1}{\sqrt{r^2 + \beta^2}} = \frac{1}{r\sqrt{1 + \frac{r^2}{\beta^2}}} = \frac{1}{\sqrt{2}r}. \tag{74}$$

Thus,

$$I = \frac{1}{\sqrt{r^2 + \beta^2}} \frac{1}{\sqrt{1 - \frac{2\beta r}{r^2 + \beta^2} \cos(\phi - \theta)}} = \frac{1}{\sqrt{2}r} \frac{1}{\sqrt{1 - h(\psi)}}, \tag{75}$$

where $h = \cos(\psi)$, $\psi = \phi - \theta$. We assume that P_0 does not collide with P_2 , implying $\psi \neq 0, \pm 2j\pi$, $j = 1, 2, 3, \dots$. Thus, $|h| < 1$. We can write I as,

$$I = \frac{1}{\sqrt{2}r}(1 + \mathcal{O}(h)). \tag{76}$$

Hence,

$$\tilde{V}_2 = -\frac{Gm_0m_2}{\sqrt{2}r} + \mathcal{O}(m_0m_2). \tag{77}$$

Proceeding as in Case 1,

$$\hat{E}_{\tilde{n}} = -\frac{2\nu\pi^2\left(Gm_0\left(m_1 + \frac{1}{\sqrt{2}}m_2\right)\right)^2}{\sigma^2\tilde{n}^2} + \mathcal{O}(m_0m_2) \tag{78}$$

This can be written as,

$$\hat{E}_{\tilde{n}} = -\frac{4\sigma}{\tilde{n}^2}\left(1 + \frac{1}{\sqrt{2}}\mu + \frac{1}{2}\mu^2\right) + \mathcal{O}(m_0m_2). \tag{79}$$

ORCID iDs

Edward Belbruno  <https://orcid.org/0000-0002-7431-9116>

References

- [1] Siegel C.L and Moser J.K 1971 *Lectures on Celestial Mechanics (Grundlehren Series)* (Heidelberg-Berlin: Springer)
- [2] Lanczos C 1949 *The Variational Principles of Physics* (Toronto: University of Toronto Press)
- [3] Pollard H 1976 *Celestial Mechanics, The Carus Mathematical Monographs* (Washington, DC: Mathematical Association of America) no. 13

- [4] Szebehely V 1967 *Theory of Orbits* (New York: Academic)
- [5] Moulton F R 1970 *An Introduction to Celestial Mechanics* (London: Macmillan) Reprinted by Dover, New York, 1970
- [6] Stiefel E L and Scheifele G 1971 *Linear and Regular Celestial Mechanics* vol 174 (New York: Springer)
- [7] Naidon P and Endo S 2017 *Rep. Prog. Phys.* **80** 056001
- [8] Belbruno E 2004 *Capture Dynamics and Chaotic Motions in Celestial Mechanics* (Princeton, NJ: Princeton University Press)
- [9] Sommerfeld A 1921 *Atombau und Spektrallinien* (Braunschweig: Friedr. Vieweg & Sohn)
- [10] Diósi L 1984 *Phys. Lett. A* **105** 199–202
- [11] Penrose R 1996 *Gen. Relativity and Gravitation* **28** 581–600
- [12] Kummer M 1979 *Am. J. Math.* **101** 1333–54
- [13] Belbruno E, Gidea M and Topputo F 2010 *SIAM J. Appl. Dyn. Sys.* **9** 1061–89
- [14] Belbruno E 1987 *Proceedings of the AIAA/DGLR/JSASS Inter. Elec. Propl. Conf.* no. 87–1054
- [15] Belbruno E, Miller J and Guid J 1993 *Control Dyn. Astr.* **16** 770–5
- [16] Belbruno E, Moro-Martin A, Malhotra R and Savransky D 2012 *Astrobiology placed after 2012* **12** 1–21
- [17] Garcia G and Gomez G 2007 *Cel. Mech. Dyn. Astr.* **97** 87–100
- [18] Llibre J, Martinez R and Simo C 1985 *J. Diff Equ.* **58** 104–56
- [19] Conley C 1968 *SIAM J. Appl. Math.* **16** 732–46
- [20] Topputo F and Belbruno E 2009 *Cel. Mech. Dyn. Astr.* **105** 3–17
- [21] Belbruno E, Gidea M and Topputo F 2013 *Qual. Theory Dyn.. Sys.* **12** 53–66
- [22] Belbruno E and Marsden B 1997 *Astron. J.* **113** 1433–44
- [23] Koon W S, Lo M W, Marsden J E and Ross S D 2001 *Celest. Mech. Dyn. Astron.* **81** 27–38
- [24] Ohtsuka K, Ito T, Yoshikawa M, Asher D J and Arakida H 2008 *Astron. Astrophys.* **489** 1355–62
- [25] Koon W S, Lo M W, Marsden J E and Ross S D 2000 *Chaos* **10** 427–69
- [26] Belbruno E, Topputo F and Gidea M 2008 *Adv. Space Res.* **42** 1330–52
- [27] Belbruno E 1997 *Annals New York Academy of Sciences (Near Earth Objects)* **822** 195–225 RemoJ New York: Wiley
- [28] Atkins P and Friedman R 2005 *Molecular Quantum Mechanics* 4th edn (Oxford: Oxford University Press)
- [29] Abramowitz M and Stegun I 1974 *Handbook of Mathematical Functions* (New York: Dover)